Demonstrating the Use of Small Uncrewed Aircraft Systems (Drones) Capabilities and Data for Iowa Transportation and Infrastructure Work

Pilot Project No. 1 – Use of Small Uncrewed Aircraft Systems for Hairline Crack Detection on Bridge Deck

Task Report | May 2025

IOWA STATE UNIVERSITY
Institute for Transportation

Sponsored by
Iowa Department of Transportation
Federal Highway Administration
SPR-RE24(010)-8H-00
(InTrans Project 24-904)

About the Program for Sustainable Pavement Engineering and Research

The overall goal of the Program for Sustainable Pavement Engineering and Research (PROSPER) is to advance research, education, and technology transfer in the area of sustainable highway and airport pavement infrastructure systems.

About the Institute for Transportation

The mission of the Institute for Transportation (InTrans) at Iowa State University is to save lives and improve economic vitality through discovery, research innovation, outreach, and the implementation of bold ideas.

Iowa State University Nondiscrimination Statement

Iowa State University does not discriminate on the basis of race, color, age, ethnicity, religion, national origin, pregnancy, sexual orientation, genetic information, sex, marital status, disability, or status as a U.S. Veteran. Inquiries regarding nondiscrimination policies may be directed to Office of Equal Opportunity, 2680 Beardshear Hall, 515 Morrill Road, Ames, Iowa 50011, telephone: 515-294-7612, email: eooffice@iastate.edu.

Disclaimer Notice

The contents of this report reflect the views of the authors, who are responsible for the facts and the accuracy of the information presented herein. The opinions, findings and conclusions expressed in this publication are those of the authors and not necessarily those of the sponsors.

This document is disseminated under the sponsorship of the U.S. DOT in the interest of information exchange. The sponsors assume no liability for the contents or use of the information contained in this document. This report does not constitute a standard, specification, or regulation.

The sponsors do not endorse products or manufacturers. Trademarks or manufacturers' names appear in this report only because they are considered essential to the objective of the document.

Quality Assurance Statement

The Federal Highway Administration (FHWA) provides high-quality information to serve Government, industry, and the public in a manner that promotes public understanding. Standards and policies are used to ensure and maximize the quality, objectivity, utility, and integrity of its information. The FHWA periodically reviews quality issues and adjusts its programs and processes to ensure continuous quality improvement.

Iowa DOT Statements

Iowa DOT ensures non-discrimination in all programs and activities in accordance with Title VI of the Civil Rights Act of 1964. Any person who believes that they are being denied participation in a project, being denied benefits of a program, or otherwise being discriminated against because of race, color, national origin, gender, age, or disability, low income and limited English proficiency, or if needs more information or special assistance for persons with disabilities or limited English proficiency, please contact Iowa DOT Civil Rights at 515-239-7970 or by email at civil.rights@iowadot.us.

The preparation of this report was financed in part through funds provided by the Iowa Department of Transportation through its "Second Revised Agreement for Management of Research Conducted by Iowa State University for the Iowa Department of Transportation" and its amendments.

The opinions, findings, and conclusions expressed in this publication are those of the authors and not necessarily those of the Iowa Department of Transportation or the U.S. Department of Transportation Federal Highway Administration.

Technical Report Documentation Page

1. Report No.	2. Government Accession No.	3. Recipient's Catalog No.
InTrans Project 24-904		

4. Title and Subtitle	5. Report Date
Demonstrating the Use of Small Uncrewed Aircraft Systems (Drones) Capabilities and Data for Iowa Transportation and Infrastructure Work: Pilot Project No. 1 – Use of Small Uncrewed Aircraft Systems for Hairline Crack Detection on Bridge Deck	May 2025 6. Performing Organization Code

7. Author(s)	8. Performing Organization Report No.
Kunle Oguntoye (orcid.org/0009-0002-9993-3304), Md Abdullah All Sourav (orcid.org/0000-0003-3387-740X), Rajrup Mitra (orcid.org/0000-0003-1937-7222), Abby Jenkins (orcid.org/0009-0007-5860-421X), Halil Ceylan (orcid.org/0000-0003-1133-0366), Sunghwan Kim (orcid.org/0000-0002-1239-2350), Berk Gulmezoglu (orcid.org/0000-0001-6268-6325), Yunjeong (Leah) Mo (orcid.org/0000-0002-5162-2235) and Colin N. Brooks (orcid.org/0000-0003-4544-2569)	InTrans Project 24-904

9. Performing Organization Name and Address	10. Work Unit No. (TRAIS)
Program for Sustainable Pavement Engineering and Research (PROSPER) Institute for Transportation Iowa State University 2711 South Loop Drive, Suite 4700 Ames, IA 50010-8664	11. Contract or Grant No.

12. Sponsoring Organization Name and Address		13. Type of Report and Period Covered
Iowa Department of Transportation 800 Lincoln Way Ames, IA 50010	Federal Highway Administration 1200 New Jersey Avenue, SE Washington, DC 20590	Task Report 14. Sponsoring Agency Code SPR-RE24(010)-8H-00

15. Supplementary Notes

Visit https://intrans.iastate.edu for color pdfs of this and other research reports.

16. Abstract

The increasing use of small uncrewed aircraft systems (sUAS), also known as drones, significantly benefits transportation agencies through reduced costs, enhanced safety, and improved productivity. The Iowa Department of Transportation (DOT) desires to use this technology in routine engineering practices, and this pilot study evaluated the effectiveness of hairline crack detection from high-resolution sUAS data collected at low altitudes. The research team collected, processed, and analyzed sUAS data on the newly constructed Northeast Mixmaster (NEMM) bridge in Des Moines, Iowa, and a one-year-old grooved-deck bridge in Humboldt County, Iowa. A DJI Mavic 2 Enterprise Advanced drone was used to collect data at 15 ft (4.6 m), 35 ft (10.7 m), and 40 ft (12.2 m) altitudes from the bridges, resulting in resolutions ranging from 0.026 in./pixel (0.66 mm/pixel) to 0.08 in./pixel (2.02 mm/pixel). The lessons learned were summarized, and recommendations for the Iowa DOT on the best practices for collecting high-resolution data from bridge decks at low altitudes were developed. The key lessons and recommendations are as follows: since manual flight takes a long time and is prone to inconsistent overlap, mid-flight altitude adjustment is required, a minimum three-person team is necessary, traffic control is crucial, and the use of portable-sized sUAS is recommended when high-resolution imagery from low-altitude flight is desired. Overall, the potential for sUAS to complement infrastructure monitoring was explored through the use of high-resolution imagery to detect structural distresses. The insights gained from this research offer valuable guidance for integrating sUAS technology into Iowa DOT practices in ways that will improve efficiency, reduce costs, and ensure safer, more effective inspections.

17. Key Words	18. Distribution Statement
crack detection—drones—drone for crack detection—infrastructure assessment— hairline crack detection—low-altitude flight—uncrewed (unmanned/unpersonned) aircraft systems	No restrictions.

19. Security Classification (of this report)	20. Security Classification (of this page)	21. No. of Pages	22. Price
Unclassified.	Unclassified.	63	NA

DEMONSTRATING THE USE OF SMALL UNCREWED AIRCRAFT SYSTEMS (DRONES) CAPABILITIES AND DATA FOR IOWA TRANSPORTATION AND INFRASTRUCTURE WORK

PILOT PROJECT NO. 1 - USE OF SMALL UNCREWED AIRCRAFT SYSTEMS FOR HAIRLINE CRACK DETECTION ON BRIDGE DECK

Pilot Project Report
May 2025

Principal Investigator
Halil Ceylan, Professor and Director
Program for Sustainable Pavement Engineering and Research (PROSPER),
Institute for Transportation, Iowa State University

Co-Principal Investigators
Sunghwan Kim, Research Scientist, Institute for Transportation, Iowa State University
Berk Gulmezoglu, Assistant Professor, Electrical and Computer Engineering, Iowa State University
Yunjeong (Leah) Mo, Assistant Professor, Civil, Construction and Environmental Engineering, Iowa State University
Colin N. Brooks, Transportation Practice Area Leader, Michigan Tech Research Institute (MTRI), Michigan Technological University

Research Associates
Md Abdullah All Sourav, Kunle Oguntoye, Rajrup Mitra, Abby Jenkins

Authors
Kunle Oguntoye, Md Abdullah All Sourav, Rajrup Mitra, Abby Jenkins, Halil Ceylan, Sunghwan Kim, Berk Gulmezoglu, Yunjeong (Leah) Mo, and Colin N. Brooks

Sponsored by
Iowa Department of Transportation and Federal Highway Administration
(SPR-RE24(010)-8H-00)

Preparation of this report was financed in part
through funds provided by the Iowa Department of Transportation
through its Research Management Agreement with the Institute for Transportation
(InTrans Project 24-904)

A report from
Program for Sustainable Pavement Engineering and Research (PROSPER)
Iowa State University
2711 South Loop Drive, Suite 4700
Ames, IA 50010-8664
Phone: 515-294-8103 / Fax: 515-294-0467
https://intrans.iastate.edu

TABLE OF CONTENTS

LIST OF FIGURES

LIST OF TABLES

ACKNOWLEDGMENTS

The authors gratefully acknowledge the Iowa Department of Transportation (Iowa DOT) for sponsoring this research and the Federal Highway Administration (FHWA) for the state planning and research (SPR) funds used for this project.

The project technical advisory committee members, Ed Bartels, Brandon Billings, Lee Bjerke, Curtis Carter, Khyle Clute, Chris Cromwell, Michelle Fields, Vanessa Goetz, Brian Keierleber, Todd Kinney, Ronald Knoche, Tim McClung, Matthew Miller, Wes Musgrove, Tammy Nicholson, Greg Parker, Jesse Peterson, Melissa Serio, Derek Snead, Cedric Wilkinson, Wade Weiss, Bob Younie, and Andrew Zimmerman, are gratefully acknowledged for their guidance, support, and direction throughout the study.

The authors acknowledge with deep appreciation the Iowa DOT's unwavering support, and this appreciation is extended to all the enthusiastic and hardworking Iowa DOT engineers and technicians who carefully carried out all field data collection. The authors would also like to express their sincere gratitude to the members of the Michigan Tech Research Institute (MTRI) research team that participated in this project and other research team members from the Program for Sustainable Pavement Engineering and Research (PROSPER) at the Institute for Transportation (InTrans) at Iowa State University (ISU) for their assistance.

EXECUTIVE SUMMARY

The increasing use of small uncrewed aircraft systems (sUAS), also known as drones, in transportation infrastructure monitoring has validated the critical importance of this technology in modern engineering practice. sUAS technology offers significant benefits, including cost efficiency, enhanced safety, and improved productivity. While these advantages align with the goals of the Iowa Department of Transportation (DOT), the integration of sUAS into routine engineering practices carried out by the Iowa DOT is yet to be fully explored.

The primary aim of this first pilot study was to evaluate the effectiveness of sUAS in distress monitoring for built structures, specifically bridges. The Iowa DOT contacted the Iowa State University (ISU) research team to explore the potential use of sUAS technology for inspecting very fine hairline cracks on two bridges: a section (Unit 1) of the newly constructed Northeast Mixmaster (NEMM) bridge in Des Moines, Iowa, and a grooved-deck bridge in Humboldt County, Iowa. The objective of the two inspections was to test the viability of the technology for detecting hairline cracks from sUAS-collected red-green-blue (RGB) imagery obtained at low altitudes.

The DJI Mavic 2 Enterprise Advanced (M2EA) sUAS was utilized for data collection. Initial data collection for the NEMM bridge involved three site visits, during which sUAS were able to capture high-resolution images at altitudes of 15 ft (4.6 m) and 35 ft (10.7 m) above ground level (AGL). The data were processed to create orthomosaics using high-accuracy ground control points. Ground sample distances (GSDs) of 0.026 in. (0.66 mm), 0.032 in. (0.81 mm), and 0.035 in. (0.88 mm) were achieved through three-part processing of the 15 ft (4.6 m) data, and a GSD of 0.066 in. (1.67 mm) was achieved for the 35 ft (10.7 m) data. Through these data collection efforts, the research team identified and measured 39 cracks on the NEMM bridge.

At the Humboldt County bridge, the data were collected at altitudes of 15 ft (4.6 m) and 40 ft (12.2 m). Detecting cracks was difficult at the Humbolt County bridge because of the grooved pavement. For the Humboldt County bridge, GSDs of 0.033 in. (0.85 mm) and 0.079 in. (2.02 mm) were achieved at altitudes of 15 ft (4.6 m) and 35 ft (10.7 m), respectively, and 9 cracks were identified and measured.

The overall recommendations, key findings, and lessons learned from this study are as follows:

- Low-altitude flights at 15 ft (4.6 m) could only be flown manually, and data collection therefore took a relatively long time. For example, it took a total of 225 minutes of flight time to cover the NEMM Unit 1 section, while the same coverage would typically have been achieved in 25 minutes if the sUAS had been flown automatically at 50 ft (15.2 m).
- Since manual flight is hard to control and prone to inconsistencies in speed and overlap, the remote pilot at the NEMM bridge site was cautious to ensure that the sUAS remained on the preplanned route and avoided flying directly above passing vehicles.
- The slope of the NEMM bridge deck made it challenging to achieve consistent resolution during flight, and mid-flight adjustment of the flight altitude was required.

- Achieving sub-millimeter accuracy is crucial for detecting fine cracks from sUAS-collected images.
- To mitigate inconsistencies during manual flight at the NEMM bridge site, the flight mode was set to "Tripod," the speed was reduced to 1 to 2 mph, and the bridge edges were marked at 6 to 7 ft (1.8 to 2.1 m) intervals to indicate crosswise reference lines for each pass.
- A flight altitude of 15 ft (4.6 m) is highly recommended when time and resources are available. To reduce data collection time without compromising data quality, it is recommended that a high-resolution camera (e.g., LR1 or Nikon D850) be deployed at higher altitudes.
- The sight of a drone in the air at the Humboldt County bridge site attracted the attention of drivers, resulting in distracted driving.
- Even with low-altitude flights, remotely detecting cracks on the grooved deck surface of the Humboldt County bridge from the orthophoto images proved challenging due to the texture and alignment of the grooves.
- A minimum of three team members is required to fulfill three roles: (1) piloting, (2) visually observing the sUAS, and (3) providing logistical support for data collection.
- It is recommended that provisions be made for multiple flight sessions by ensuring that a power source is available for charging on site.

This study resulted in specific key findings, lessons learned, and recommendations based on the data collection activities at the selected bridges and the final analysis of the data. Overall, the study explored the potential for sUAS to complement infrastructure monitoring through the use of high-resolution imagery to detect structural distresses. The insights gained from this research offer valuable guidance for integrating sUAS technology into Iowa DOT practices in ways that will improve efficiency, reduce costs, and ensure safer and more effective inspections.

1. INTRODUCTION

1.1. Background and Problem Statement

The extensive use of small uncrewed aircraft systems (sUAS), commonly known as drones, in the transportation industry for remote sensing and infrastructure monitoring has validated the critical importance of this technology in modern engineering practice (Watts et al. 2012). This technology has been adopted by both government agencies and private entities responsible for highways, bridges, transportation infrastructure, and airports (Banić et al. 2019, Fischer et al. 2020, Flammini et al. 2016, Nooralishahi et al. 2021, Pietersen et al. 2022, Tan and Li 2019).

For example, a wide variety of studies have been conducted on airfield pavement damage detection and rating and on the long-term use of sUAS to complement traditional pavement inspection processes (Pietersen et al. 2022, Sourav et al. 2023, Sourav et al. 2024a, Sourav et al. 2022a, Sourav et al. 2022b, Sourav et al. 2022c, 2024b, Sourav et al. 2022d, Vidyadharan et al. 2017). These studies have also provided guidelines for adoption and have explored future potential applications (Sourav et al. 2023, Sourav et al. 2024a). In addition, multiple studies in the United States and China have reported on the use of sUAS for highway and local road inspection, particularly for damage detection and ride quality index calculations (Fischer et al. 2020, Leonardi et al. 2019, Moon and Lee 2022, Peddinti et al. 2023, Quinton and Regan n.d., Roberts et al. 2020). sUAS technology is also increasingly being used for railway infrastructure inspection, enabling efficient monitoring of tracks, bridges, and overhead structures. Studies have demonstrated its effectiveness in detecting track defects, inspecting tunnels, and assessing vegetation encroachment, all of which reduce the need for manual inspections and minimize service disruptions (Aela et al. 2024, Banić et al. 2019, Flammini et al. 2016).

Bridge inspections, especially in hard-to-reach areas, have also been conducted using sUAS (Escobar-Wolf et al. 2018, Feroz and Abu Dabous 2021, Pokhrel et al. 2024, Seo et al. 2018, Tomiczek et al. 2019). These systems offer close-up visual inspection capabilities and an added layer of safety by mitigating the risks associated with slips, trips, falls, and overexertion. Furthermore, they help prevent injuries and illnesses caused by exposure to hazardous animals (e.g., snakes, falcons, raccoons) and toxic plants (e.g., poison ivy, poison oak, thorns) (BLS 2019, Hubbard et al. 2017). Based on past and current trends, sUAS technology offers numerous benefits, including cost optimization, enhanced safety, and improved productivity (McGuire et al. 2016).

While these advantages align with the goals of the Iowa Department of Transportation (Iowa DOT), questions remain regarding how best to integrate sUAS technology into routine engineering practices. Inspecting transportation infrastructure is a routine task performed by state department of transportation (DOT) engineers to assess structural health and plan maintenance schedules. Traditionally, these inspections have been conducted manually, requiring significant resources in terms of personnel, cost, and time while ensuring safety and minimizing traffic disruption (Sattar et al. 2018). Given the challenges of balancing these priorities, sUAS technology presents a promising solution.

1.2. Goal and Objectives

The overarching goal of this pilot study was to evaluate the use of sUAS as a monitoring tool for road and bridge infrastructure, particularly for detecting fine-resolution distresses that are difficult to identify manually. The study focused on automating distress monitoring for built structures.

The specific objective of the study was to investigate the feasibility of detecting hairline cracks in bridges from red-green-blue (RGB) data collected during low-altitude sUAS flights and to provide technical guidelines, recommendations, and best practices for wide-scale adoption. The research team collected, processed, and analyzed RGB data from two sites requested by the Iowa DOT: the newly constructed Northeast Mixmaster (NEMM) bridge at the intersection of I-235 and I-80 in Des Moines, Iowa, and a grooved-deck bridge in Humboldt County, Iowa. Due to the presence of hairline cracks on both bridges, the research team experimented with collecting high-resolution RGB imagery at altitudes of 15 ft (4.6 m), 35 ft (10.7 m), and 40 ft (12.2 m) above ground level (AGL). It was observed that while lower flight altitudes provide finer spatial resolution, other critical factors must be considered before and during data collection flights.

This report provides details on the research activities and highlights the key findings, lessons learned, and recommendations resulting from the study, covering aspects from the data collection pipeline to final data analysis and remote sensing applications.

2. NEMM BRIDGE INSPECTION

The research team hosted a project kickoff meeting on September 13, 2024, to discuss the background and goals of the pilot studies and possible tasks to be completed as part of the awarded research project. Based on discussions at the kickoff meeting, a collaborative effort was initiated between the research team and the Iowa DOT, represented by Cedric Wilkinson and Jesse Peterson.

The first pilot study decided upon in the meeting was to collect sUAS-based data to document and assess bridge deck cracks on a section of the newly constructed NEMM bridge located at the intersection of I-235 and I-80 north of Des Moines, Iowa, as shown in Figure 1. The area in the figure enclosed by the yellow line indicates the location where the new bridge was constructed. The bridge is divided primarily into three sections: Unit 1 (west section), Unit 2 (middle section), and Unit 3 (north section), with only Unit 1 open for data collection by the research team. Unit 1 of the bridge is about 1,140 ft (347.5 m) long and 48 ft (14.6 m) wide. Some longitudinal and transverse cracks began appearing on the bridge deck after construction, prompting the Iowa DOT to engage Niricson, a private consultant, and later Iowa State University (ISU) to document cracks in the bridge deck using sUAS. Niricson initially collected sUAS-based data from the Unit 2 and Unit 3 sections of the bridge deck. These sections had relatively large visible cracks and were subsequently overlaid to address immediate structural concerns. In contrast, Unit 1 was built with a different concrete mix, and the cracks in this section were finer than those in the other units. The Iowa DOT was particularly interested in the viability of using sUAS to document cracks on the Unit 1 bridge deck.

Figure 1. Location of the newly constructed NEMM bridge at the I-235 and I-80 intersection north of Des Moines, Iowa

The ISU research team made three visits to the data collection site during September 2024 and October 2024. The first visit was a preliminary bridge and under-bridge visual inspection, with Iowa DOT staff seeking ideas on developing data collection plans. On the second and third visits, tasks included sUAS-based data collection, physical measurement, and documentation of several cracks from the Unit 3 section of the bridge deck. The ISU research team used the DJI Mavic 2 Enterprise Advance (M2EA) sUAS shown in Figure 2 for high-resolution RGB data collection with a 48 MP "quad-bayer" visual RGB camera. The team also used 10 Global Positioning System (GPS)-enabled Propeller AeroPoints ground control points (GCPs) for recording centimeter-level positional data that were used in post-processing the sUAS data to produce highly accurate orthophotos. The data were collected at 15 ft (4.6 m) AGL and 35 ft (10.7 m) AGL and were then used to create RGB or "natural color" orthophotos, digital elevation models (DEMs), and grayscale three-dimensional (3D) terrain representations (or hillshades) from the DEMs. Details regarding the study objective and the data collection, processing, and analysis activities are provided in the following sections.

Figure 2. DJI Mavic 2 Enterprise Advance sUAS

2.1. Objective

The primary objective of the data collection was to collect high-resolution RGB data to comprehensively document cracks and evaluate the efficacy of this method for detecting hairline cracks.

2.2. NEMM Bridge Field Data Collection

2.2.1. NEMM Bridge Data Collection – Preliminary Inspection

The preliminary inspection began with the ISU research team's on-site assessment of the bridge on September 26, 2024, guided by Jesse Peterson, Iowa DOT Structures Field Engineer. This initial visit allowed the team to evaluate the layout of the bridge and the locations and types of cracks present, providing essential context for the detailed data collection to follow. Based on the initial evaluation and comments from Jesse Peterson, it was determined that at the Unit 1 section, or the west end, the bridge had a superelevation or transverse slope of 4% to 6% and a gradient

or longitudinal slope of about 3% to 4%. The highest point of the bridge was about 75 ft (22.9 m). The preliminary inspection showed that Unit 1 was still not milled at that point in time and had the finest cracks, as shown in Figure 3. Though many of the cracks were long, their widths ranged between approximately 0.004 in (0.1 mm) and 0.012 in (0.3 mm). Most cracks were not visible in direct sunlight but became detectable under shadow or when water was applied to the surface. Close inspection was necessary to observe these fine cracks accurately. Unit 2, or the middle section, was already milled, so the cracks were mostly not visible, as shown in Figure 4. Unit 3, or the north section, had larger cracks, though most had been overlaid. Niricson had already collected data from this section. The team also inspected the area beneath the bridge from the north end, where Jesse Peterson pointed out large transverse cracks visible from below, as shown in Figure 5. These cracks appeared to be expanding upward through the structure, leading to the exposure of the cracks on the bridge surface.

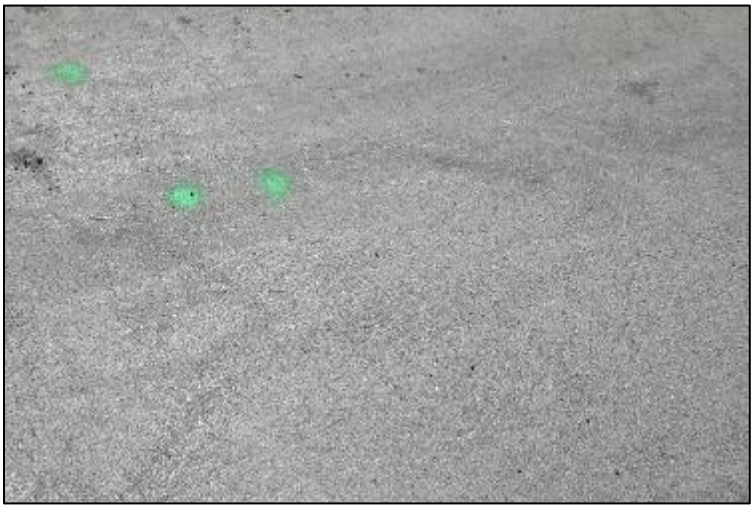

Figure 3. Cracks found in Unit 1

Figure 4. Milled surface of Unit 2

Figure 5. Cracks underneath the north side of the bridge

Some of the crucial conclusions from the day's initial inspection obtained from discussions within the research team were as follows:

- Unit 1 had the finest cracks among all three sections and needed to be inspected. Unit 2 and Unit 3 did not need to be inspected.
- The data collection needed to be completed within a week before Unit 1 was to be milled.
- Due to the minimal transverse slope and the shorter width in Unit 1, a lateral flight plan seemed optimal.
- Some potential logistical challenges were the presence of heavy construction equipment and ongoing construction activities, shown in Figure 6, and high wind conditions.
- The sUAS flight altitudes were set at 15 ft (4.6 m) and 35 ft (10.7 m), aiming for an approximate ground sample distance (GSD) of 0.04 to 0.06 in (1 to 1.5 mm).
- Since the area fell under Class E airspace, it had a maximum auto-authorized admissible flying limit of 100 ft (30.5 m), as shown in Figure 7. A Low Altitude Authorization and Notification Capability (LAANC) clearance from the Federal Aviation Administration (FAA) was required.
- It was initially planned that data be collected on September 30, 2024, and that the entire task be completed in one day.
- Based on the information provided by Jesse Peterson that the bridge deck would be cleaned on September 30, 2024, the data collection flights were rescheduled to October 1, 2024.

Figure 6. Presence of heavy construction equipment

Figure 7. LAANC map with maximum approved flying heights shown in feet

This preliminary assessment helped the team plan a more precise approach for the full inspections, ensuring that the necessary data could be gathered despite environmental and structural challenges.

2.2.2. NEMM Bridge Data Collection – Day-1

October 1, 2024, began with the ISU research team meeting Jesse Peterson at the Driver's License Station in Ankeny, Iowa, and then heading to the construction site. The objective of the day was to complete end-to-end precise sUAS-based data collection and perform a manual inspection of the Unit 1 section to identify, measure, and document cracks. After reaching the site, the team held a stand-up meeting led by the head pilot-in-command (PIC), Md. Abdullah All Sourav. The meeting was to provide a safety briefing to go through all of the tasks involved in the data collection, such as the role of the visual observer (VO), logistics and documentation, flight logs, manual inspection, measurements, and crack documentation.

With the preflight planning complete, the team ensured that the bridge section was free of obstacles and ready for operation. The research team placed 10 GPS-enabled Propeller AeroPoints GCPs at intervals along both sides of the bridge in the longitudinal direction, as shown in Figure 8. The AeroPoints automatically collected highly accurate GPS data that were uploaded to Propeller's cloud server and used for sUAS data processing to improve merged imagery outputs. For the initial few flight operations, an M2EA Real-Time Kinematics (RTK) module was used for better geo-positioning and stability using Networked Transport of RTCM via Internet Protocol (NTRIP). However, each time the sUAS and its remote controller were shut down and restarted for a battery change, the RTK module had issues connecting to the NTRIP server, so onboard GPS was used for position in the later flights.

Figure 8. Placement of AeroPoints GCPs on the ground

As previously decided, sUAS flights were to be conducted at altitudes of 15 ft (4.6 m) and 35 ft (10.7 m), targeting an approximate GSD of 0.04 to 0.06 in (1 to 1.5 mm) or lower. Since the M2EA cannot be flown on autopilot below 40 ft (12.2 m), the sUAS had to be manually flown. Due to such low flying altitudes and the desire to achieve higher stability during data collection, the "Tripod" flight mode was activated every time during the data collection phase, allowing the flight speed to be kept at less than 2 mph (0.9 m/s). The "Positioning" flight mode was used for moving the sUAS from one part of the bridge to another or taking a quick look at specific parts of the bridge. The data collection team initially tried to collect data by flying the M2EA along the bridge section but later decided to fly across the bridge deck to maintain a stable straight-line flight for adequate forward and side overlap for the entire 15 ft (4.6 m) altitude data collection. To achieve an appropriate overlap between passes, markings were made at an interval of approximately 6.5 ft (1.9 m), as shown in Figure 9.

Figure 9. Markings at intervals of about 6.5 ft for an appropriate overlap

Each flight mission covered a segment of Unit 1 and lasted up up to 20 minutes based on weather conditions and battery performance. The VO maintained communication with the PIC throughout each flight to ensure safe and uninterrupted operations. In parallel with data collection, a teammate performed a manual inspection of the bridge deck to identify crack locations that were then measured and documented, as shown in Figure 10 and Figure 11. This marking process provided essential ground truth data to support subsequent crack visibility analysis. A total of 13 cracks were marked, measured using a crack width gauge, and documented during the first day of the data collection, resulting in crack width measurements varying from 0.006 in (0.15 mm) to 0.028 in (0.7 mm). The research team also poured water onto the concrete to make some of the cracks more visible (Figure 11).

Figure 10. Crack width gauge being used to measure the width of a crack accurately

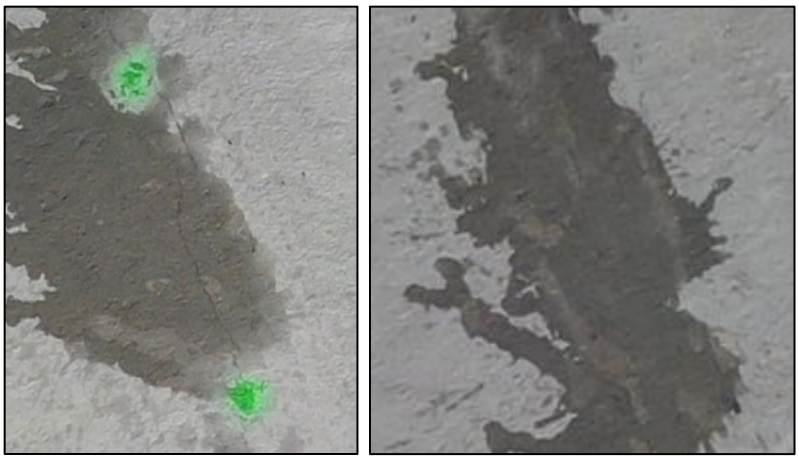

Figure 11. Water poured onto the concrete for crack visibility enhancement

The team faced challenging environmental conditions, with strong winds of 14 to 18 mph (6.3 to 8.1 m/s) and high gusts, leading to difficulty in sUAS control. The flights were unstable, causing the sUAS to shake, complicating manual control and requiring constant adjustment to maintain stable flight paths. The slope variability and elevation changes in the surface of Unit 1 added to the complexity, necessitating a careful approach to sUAS navigation to ensure that all target areas were covered without missing critical details. Due to heavy traffic in the area and the strong wind conditions, flight operations in the afternoon were deemed unsafe, leading to the decision to suspend flights for the day. Figure 12 and Figure 13 show data collection activities.

Figure 12. PIC controlling the sUAS while the VO keeps a close watch on the sUAS and the surrounding area

Figure 13. sUAS being navigated near the edge of the bridge to ensure that all target areas are covered precisely

Despite the challenging conditions, the team successfully completed a significant part of the data collection, capturing extensive imagery and GPS data for further analysis. For the day, the sUAS was flown at a flying altitude of 15 ft (4.6 m) over a section of 420 ft (128.0 m) in length and 65 ft (19.8 m) in width. A GSD ranging from about 0.025 in (0.64 mm) to about 0.032 in (0.81 mm) was achieved while flying manually. A total of 2,168 RGB images and 2,168 thermal images were collected through 68 passes made during the flight missions, as shown in Figure 14. After discussions with Jesse Peterson and considering weather, site accessibility, and the need to collect data before Unit 1 was milled, it was decided to proceed with data collection on October 3, 2024.

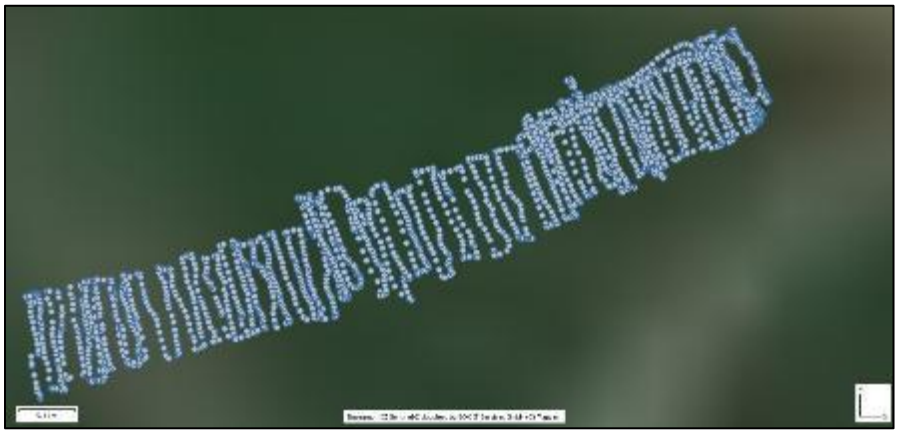

Figure 14. sUAS image points

Some of the crucial conclusions and challenges from the day's data collection were as follows:

- Wind speeds reached higher than 14 mph, with heavy gusts.
- Flight stability was compromised, causing significant movement of the sUAS.
- Landing procedures were challenging due to wind conditions.
- Mid-flight deviations occurred frequently.

- Flights were suspended in the afternoon.

2.2.3. NEMM Bridge Data Collection – Day-2

The research team returned to the NEMM bridge site in Des Moines, Iowa, on October 3, 2024, to complete the inspection of Unit 1. Favorable weather conditions, including relatively low wind speeds ranging from 6 to 13 mph (2.7 to 5.8 m/s), clear sunny skies, and a high temperature of 83°F, ensured safe sUAS mission flights. The team conducted routine safety checks by assessing the flight vicinity to ensure that it was free of hindrances. After a stand-up meeting among the team members, the team placed Propeller AeroPoint GCPs at intervals on both sides of the bridge.

Before takeoff, the team performed a quick manual inspection of the bridge deck, identifying the locations of crack distresses to be marked and measured. Figure 15 shows a team member measuring a hairline crack using a crack gauge. Observing these cracks helped create ground truth data samples used for visibility analysis in later sections. The main data were collected at 15 ft (4.6 m) AGL, and additional data were collected at 35 ft (10.7 m) AGL. Data collection for the remaining Unit 1 sections at 15 ft (4.6 m) AGL was completed using seven separate manual flights. Figure 16 illustrates the combined paths of the seven missions.

Figure 15. Ongoing measurement of observed hairline cracks

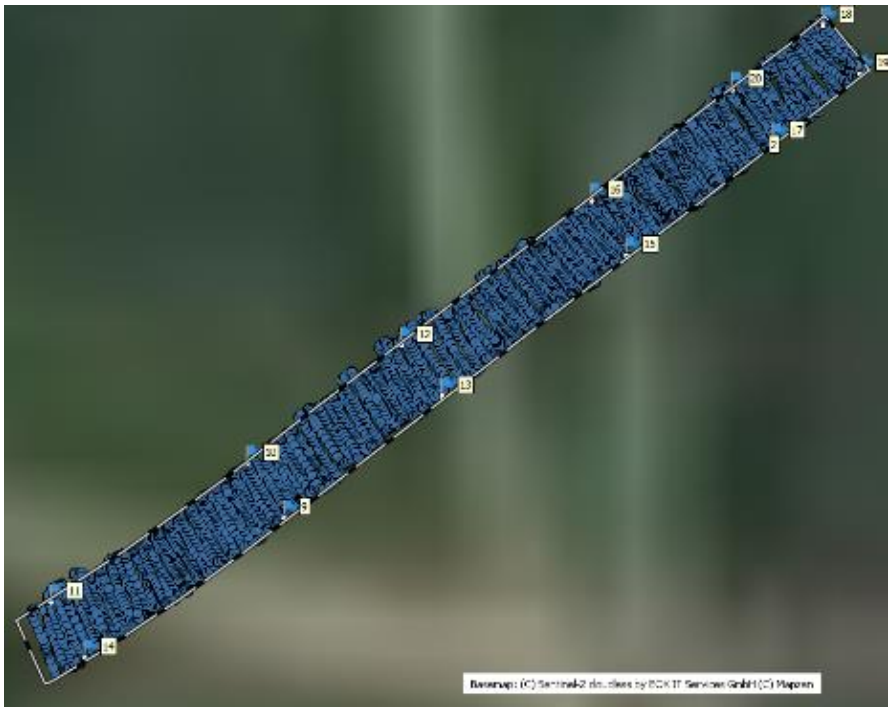

Figure 16. sUAS image points and GCPs represented using white boxes

2.3. Data Processing

The data collected from the NEMM bridge were processed in different sets within Agisoft Metashape, a widely used close range photogrammetry software package. A computer equipped with an Intel Xeon W-2265 processor (19.25M cache, 3.50 GHz) with 12 cores and 24 threads, 128 GB DDR4 ECC RAM, and an NVIDIA QUADRO RTX 5000 16 GB graphic card with 3,072 CUDA cores was used for this processing. The sUAS data collected at 35 ft (10.7 m) AGL were processed as a single set in Agisoft Metashape. Eight GCP locations were used to correct image location information. The times required to process the dataset are provided in Table 1. Processing of the sUAS data collected at a 15 ft (4.6 m) altitude was attempted in two groups: data collection on day 1 and data collection on day 2. However, since a small portion of the day 1 data collected before suspending the data collection had inconsistent GPS information and did not align properly in the software, the smaller part was processed separately. Each dataset processing session consisted of a few standard steps described below. A total of 20 GCPs were used for all data collected at 15 ft (4.6 m) AGL.

Table 1. NEMM bridge data collection and processing details

Section	Images	Capture Time (mins)	Time Required (mins)					GSD (in. (mm))
			Alignment	Depth Maps	Model	Ortho	Total	
15 ft part 1	1,730	80	31	789	212	468	1,500	0.032 (0.81)
15 ft part 2	184		9	22	15	11	57	0.026 (0.66)
15 ft part 3	3,362	110	162	598	150	266	1,176	0.035 (0.88)
35 ft part 3	529	35	21	35	302	35	393	0.066 (1.67)

Image alignment was the first step in creating orthomosaics from RGB optical data. This process involves matching key points across overlapping images to determine the relative position of each photo. To ensure high-accuracy alignment, key point limits of 40,000 and tie points of 10,000 were selected as the parameters for all image processing. After image alignment was completed, the research team created a point cloud, a set of data points that represents the surface of an object in 3D space. Each point in the cloud corresponds to a spatial measurement on the pavement surface defined by x, y, and z coordinates. This collection of points provides a detailed 3D representation of the object, capturing its shape and spatial features. The point cloud is generated using a dense map, and in this case, medium quality with mild filtering was used during point cloud generation.

The research team subsequently generated a polygonal-mesh model based on the dense cloud created during point cloud generation, targeting medium quality and a high face count, which allowed for a detailed and accurate 3D model that would capture complex surface features. Finally, an orthomosaic image, a detailed, high-resolution raster created by stitching together many drone images into a seamless image, was created. Orthomosaics were created using the default mode in Agisoft Metashape. The orthophotos were then exported to the projected coordinate system of NAD83(2011)/UTM zone 15N for better viewing and accurate projection. The details regarding the number of images, flight time for capture, processing time, and GSD are outlined in Table 1. Snapshots of the orthophotos are also provided in Figure 17 through Figure 21.

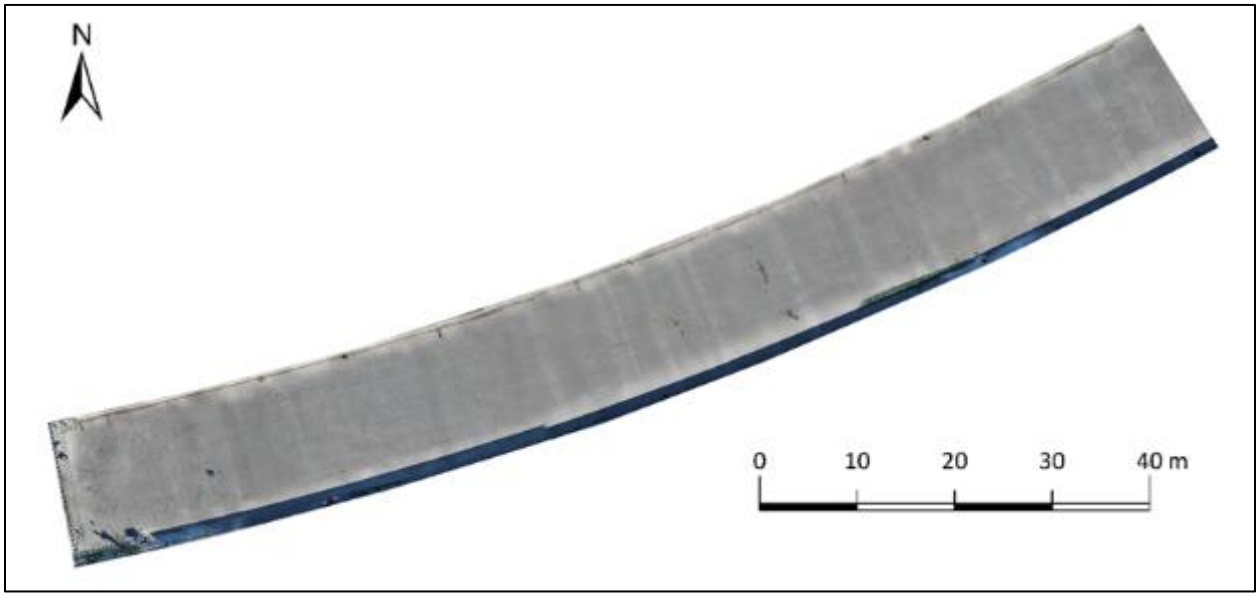

Figure 17. Part-01 15 ft orthoimage

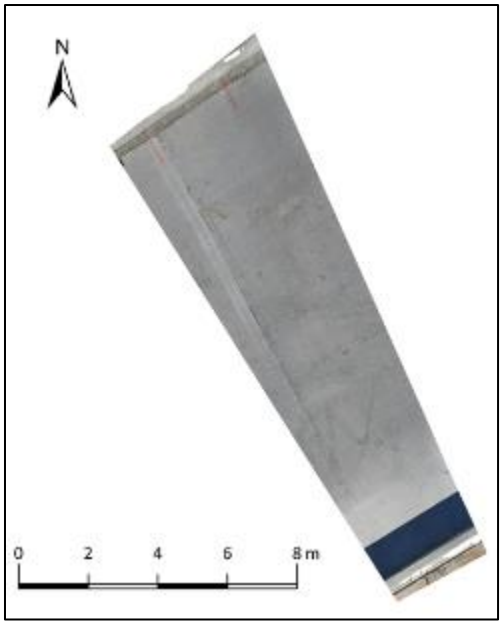

Figure 18. Part-02 15 ft orthoimage

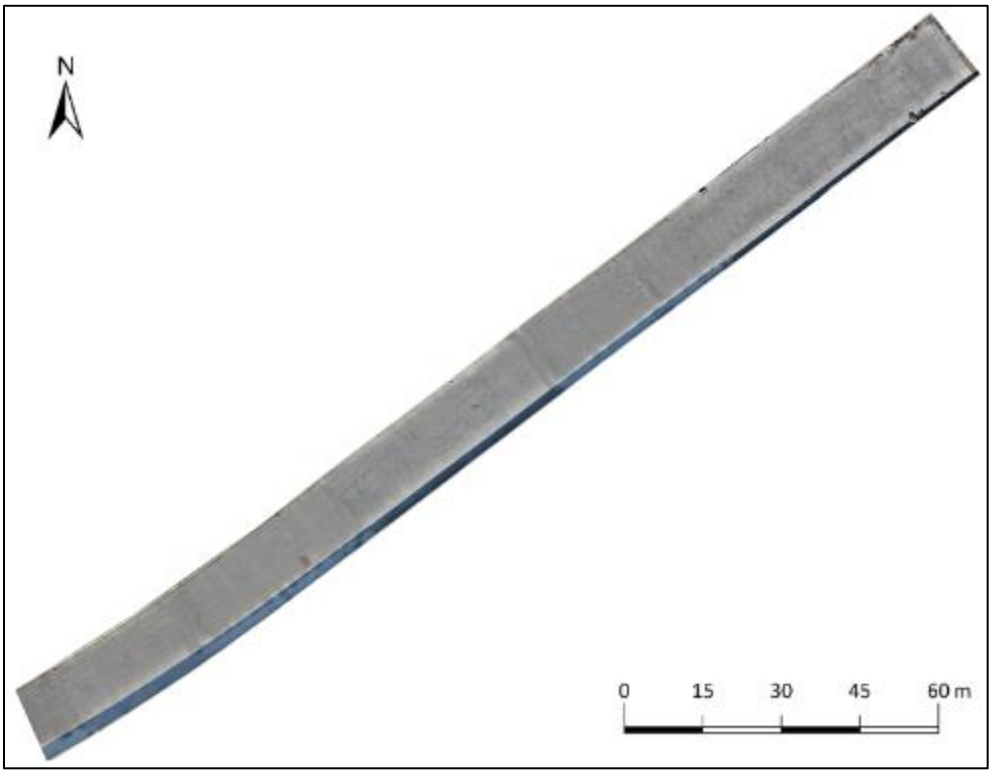

Figure 19. Part-03 15 ft orthoimage

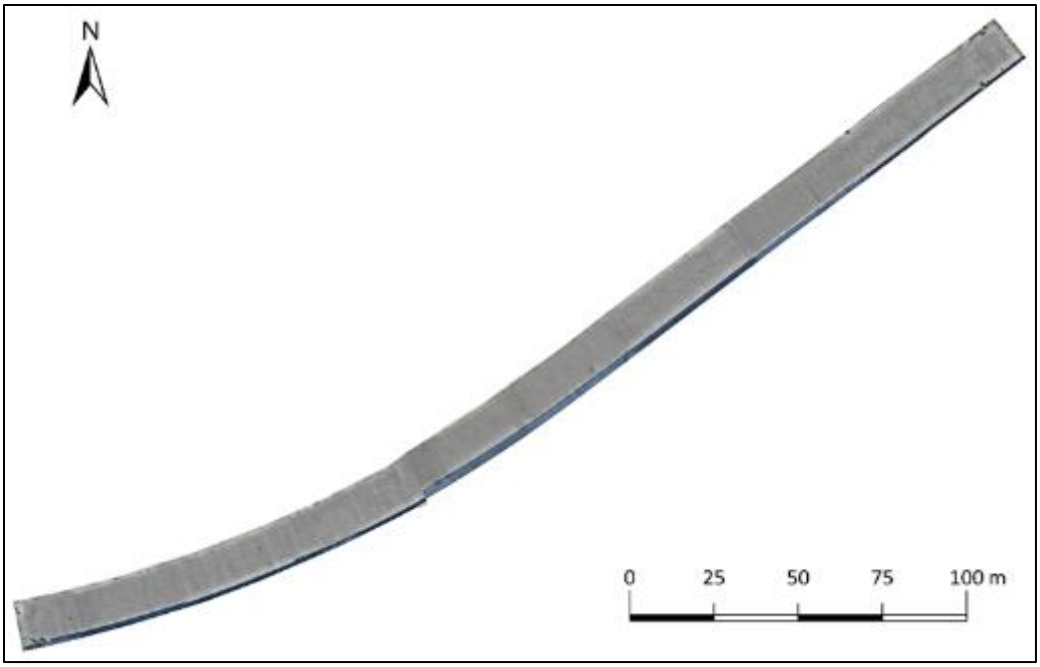

Figure 20. Combined Part-01 to Part-03 15 ft orthoimage

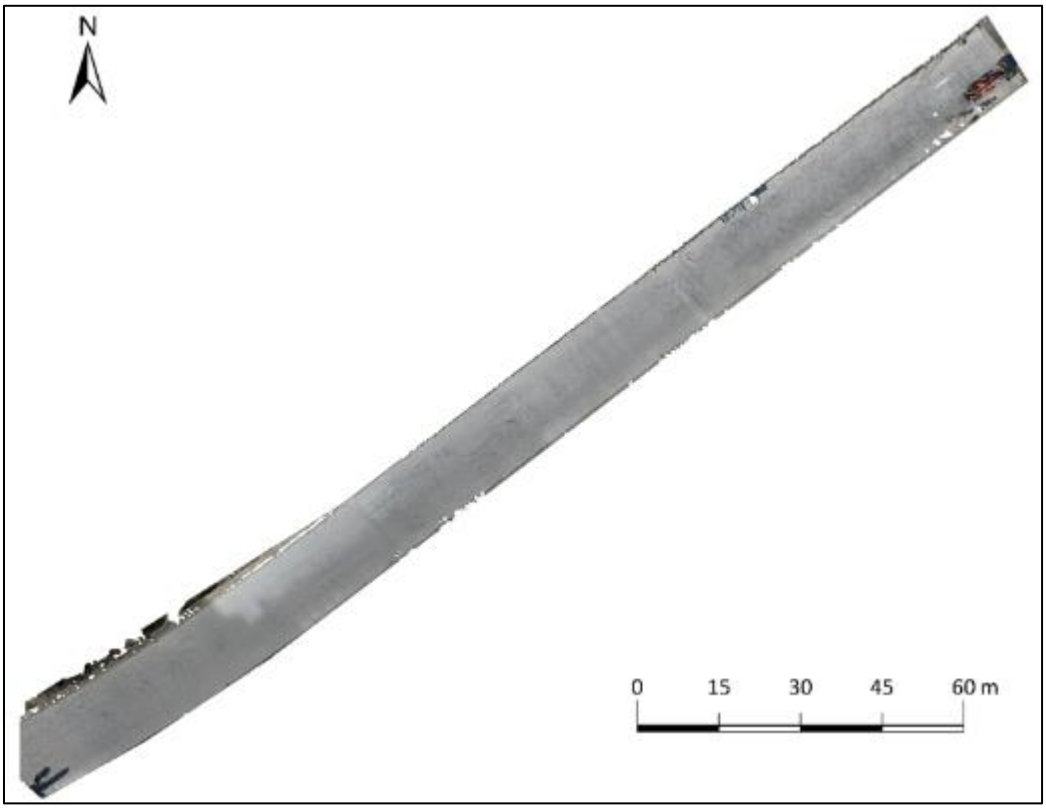

Figure 21. Part-03 35 ft orthoimage

2.4. Data Analysis

For analysis, the research team explored the visibility of the 39 identified ground truth hairline cracks from the initial manual survey, with identified cracks marked using colored spray and chalk for clarity and proper referencing. Of the 39 total cracks, 8 were marked on the first data collection day, and the remaining 31 were marked on the second day. In addition to marking each crack with spray and chalk, the research team labeled every crack uniquely to enable further analysis and aggregation. This section discusses the visibility analysis of these marked cracks in the processed orthophotos obtained from sUAS flights conducted at altitudes of 15 ft (4.6 m) and 35 ft (10.7 m) AGL.

Sections of the marked cracks in the orthophoto images were exported from ArcGIS Pro, and, to account for resolution differences, a scale value of 1:2.5 was applied to the 15 ft (4.6 m) orthophotos and a scale value of 1:4 was applied to the 35 ft (10.7 m) AGL orthophotos. While the exported images were used for extended image processing, the research team asked four reviewers who had not seen the cracks or been to the bridge to categorize the difficulty of detecting the cracks from the complete orthoimage using a guide template. The detection task was standardized by first setting the initial view scale to 1:4 and then asking reviewers to judge whether a crack was visible from the initial scale and to take note of the time and any additional effort expended in detecting the cracks. This guiding template helped reviewers categorize the level of detection as easy, moderate, or difficult as follows:

- Categorize as “easy” if the crack is identified from the baseline scale without any additional zooming and within 10 seconds. (An “easy” designation is mapped to 1.)
- Categorize as “moderate” if the crack is detected within 30 seconds and with minimal zooming. (A “moderate” designation is mapped to 2.)
- Categorize as “difficult” if the crack is found after 30 seconds and with multiple rescaling attempts. (A “difficult” designation is mapped to 3.)
- Otherwise, categorize as “not visible.” (A “not visible” designation is mapped to 4.)

The reviewers’ labels were aggregated, weighted, and compared for further analysis. Since the reviewers were knowledgeable about cracks but had no prior knowledge of the exact crack locations in the bounded marks, their deductions were assigned more weight. The final aggregate score was defuzzified using the numerical range illustrated in Figure 22. Table 2 shows the final weighted detection level for each crack sample and the combined similarity counts of the reviewers (4) and the sUAS team (1).

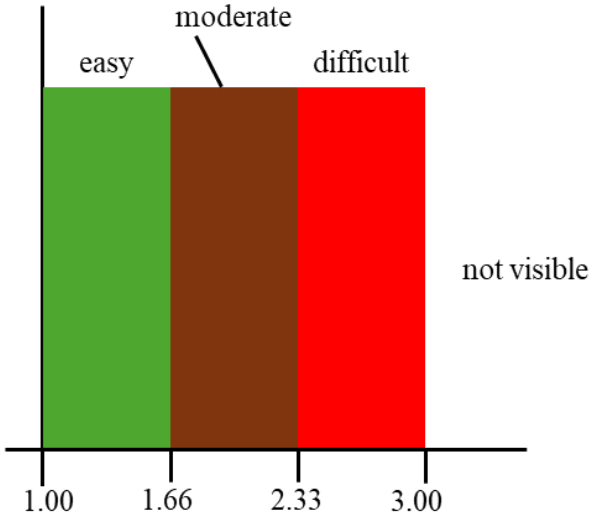

Figure 22. Final level of detection bounding range

Table 2. Sample of aggregated reviews and final score for 15 ft (4.6 m) AGL data

Crack ID	Easy	Moderate	Difficult	Not Visible	Final
1	4	1	0	0	easy
2	2	2	1	0	easy
3	3	2	0	0	easy
4	5	0	0	0	easy
5	3	2	0	0	easy
6	0	1	0	4	not visible
7	2	0	1	2	difficult
8	5	0	0	0	easy

To further improve understanding of the quality of the resulting orthoimages, the exported images were grouped into four major categories based on two image characteristics: light intensity and texture. Shadow and no-shadow represented light intensity in the image, with shadow indicating low light intensity and no-shadow indicating high light intensity. Rough and smooth were related to surface texture, with rough indicating more textured surfaces and smooth representing fewer textured surfaces. Since each image uniquely belonged to one of the subgroups of the two image characteristics, the classes were combined for every image, resulting in four final classes: smooth-shadow, smooth-no-shadow, rough-shadow, and rough-no-shadow.

Further analysis and comparison of the image classes with the detection levels provided insight into the conditions potentially influencing hairline crack detection in orthophoto images. The counts of individual and combined image classes are shown in Figure 23 and Figure 24, respectively. The increase in the number of smoother images collected at 35 ft (10.7 m) AGL was likely a result of lower image resolution. There were also more no-shadow images in the 35 ft (10.7 m) AGL data compared to the 15 ft (4.6 m) AGL data due to the time difference in data collection. The image class distribution in Figure 24 reveals that 18 out of 31 images fell under

the rough-no-shadow class, underscoring the ability of the fine resolution data obtained by the 15 ft (4.6 m) AGL orthophotos to capture the detailed texture of the concrete surface.

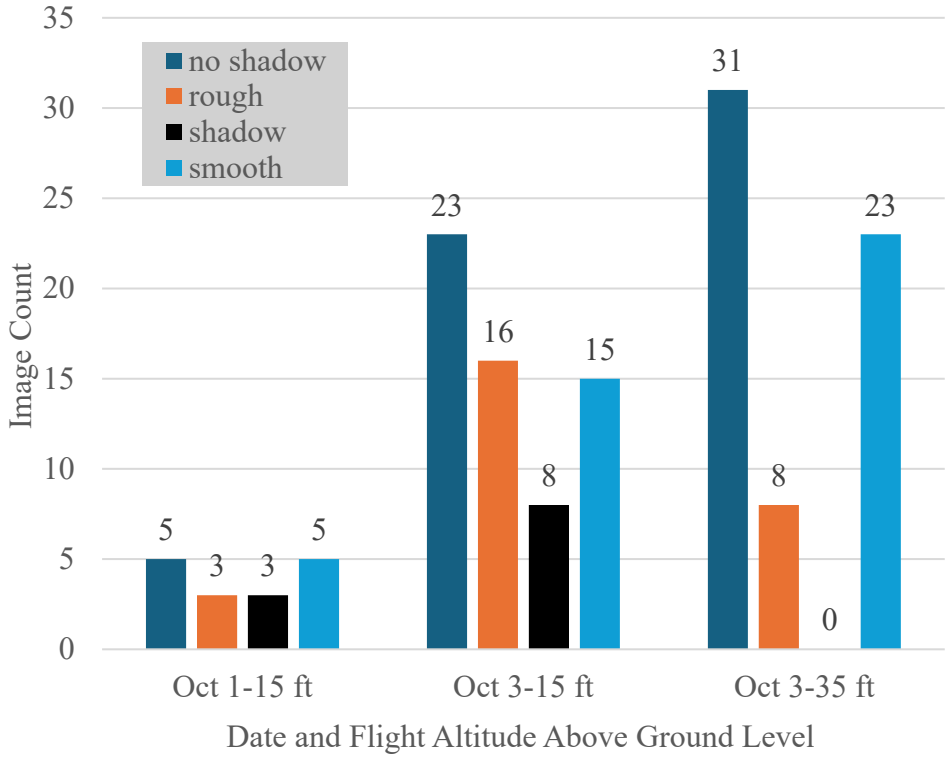

Figure 23. Counts of image classification clusters

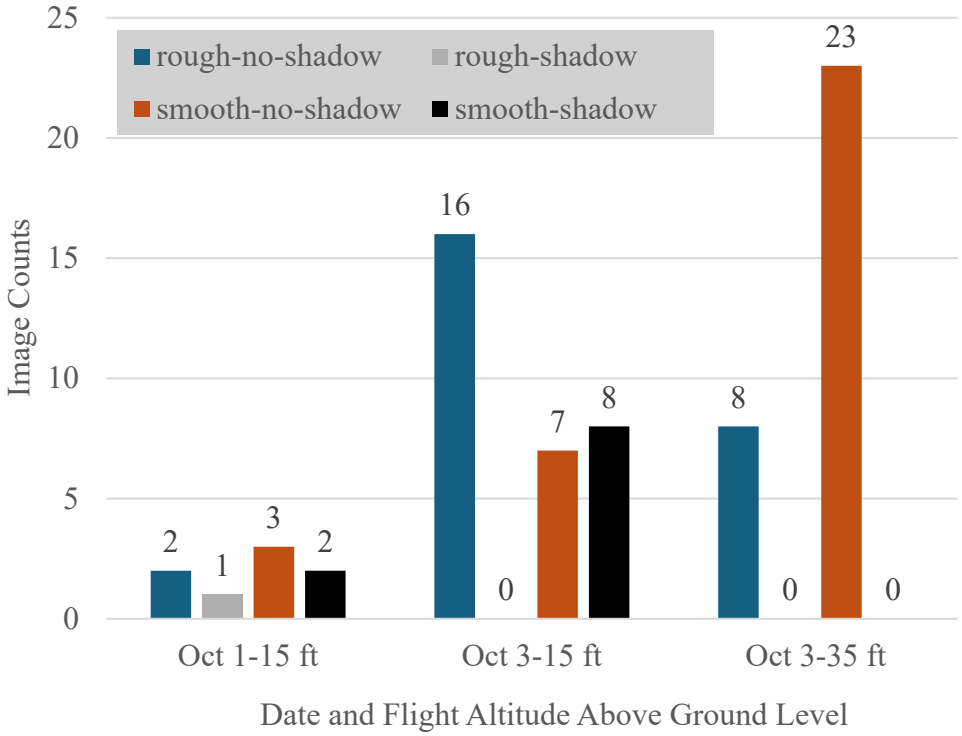

Figure 24. Counts of combined image classification clusters

Since the sUAS was flown at 15 ft (4.6 m) AGL on both inspection days and at 35 ft (10.7 m) AGL on only the second inspection day, the complete dataset of 39 ground truth cracks is available for the 15 ft (4.6 m) AGL orthophotos, while only 31 cracks are available for the 35 ft (10.7 m) AGL orthophotos. Figure 25 illustrates the number of detected or visible hairline cracks in the orthophoto images based on the reviewers' aggregation, grouped by collection date and sUAS flight altitude. The research team concluded that hairline crack detection is more challenging in 0.066 in./pixel (1.67 mm/pixel) orthophotos collected at 35 ft (10.7 m) AGL due their smoothness and lower resolution. Only 4 of the 31 available cracks were detected.

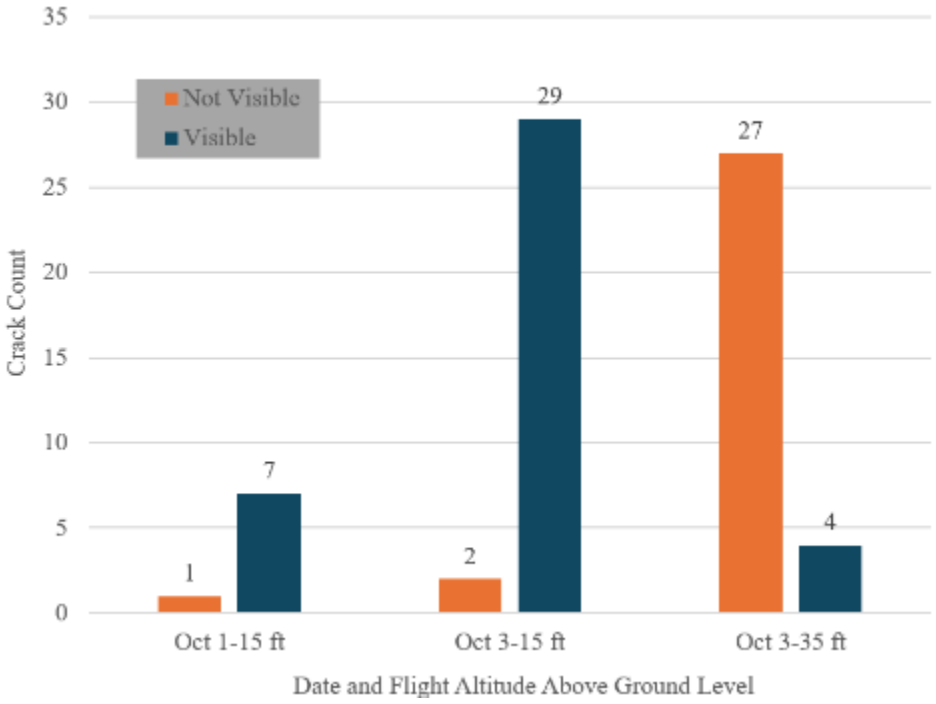

Figure 25. Visible and not-visible hairline cracks from exported RGB orthophoto images at 15 ft (4.6 m) and 35 ft (10.7 m) flight altitude

Figure 26 shows a histogram of the distribution of the measured crack widths, while Table 3 summarizes the descriptive statistics of the crack widths. Based on the histogram plotted in Figure 26, approximately 66.67% of the ground truth samples have crack widths between 0.0079 and 0.0106 in (0.2 and 0.3 mm), further highlighting the significant number of fine/hairline cracks.

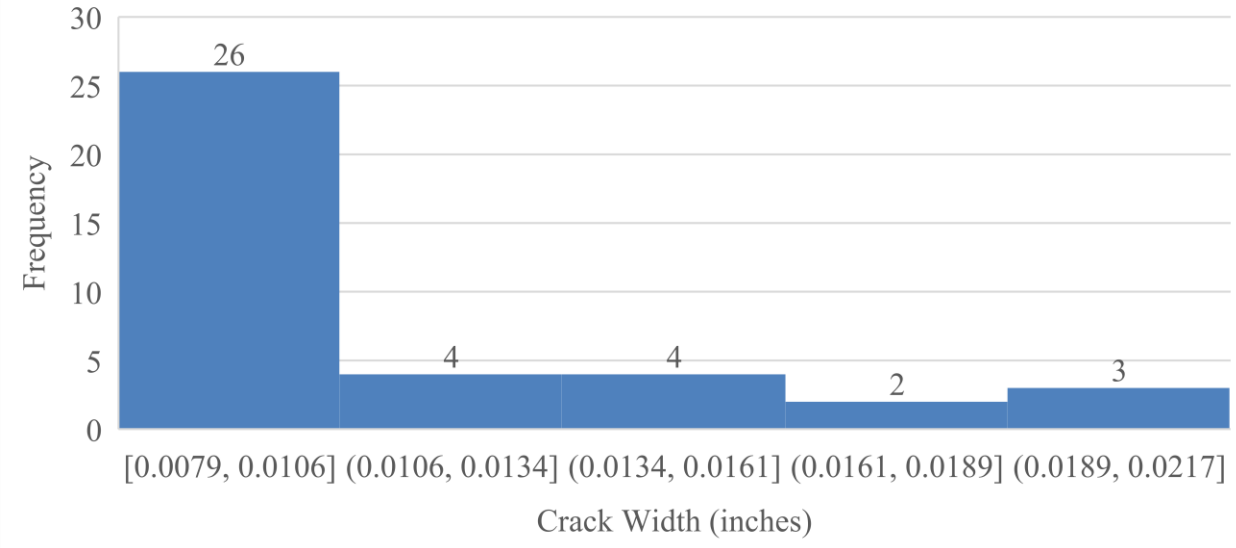

Figure 26. Histogram plot of measured crack widths

Table 3. Summarized crack width statistics in inches

Minimum	Maximum	Average	Standard Deviation
0.0079	0.0217	0.0109	0.0040

Given the greater detection success for the 15 ft (4.6 m) AGL images, the final attributed labels for the 15 ft (4.6 m) AGL crack images were further analyzed to identify factors influencing hairline crack detection in orthophoto images. Figure 27 provides an overview of detection levels for all images with visible cracks. The detected cracks from the first-day images were classified as easy (6) or difficult (1), while the majority (24 out of 29) of the detected cracks in the second-day images were classified as easy.

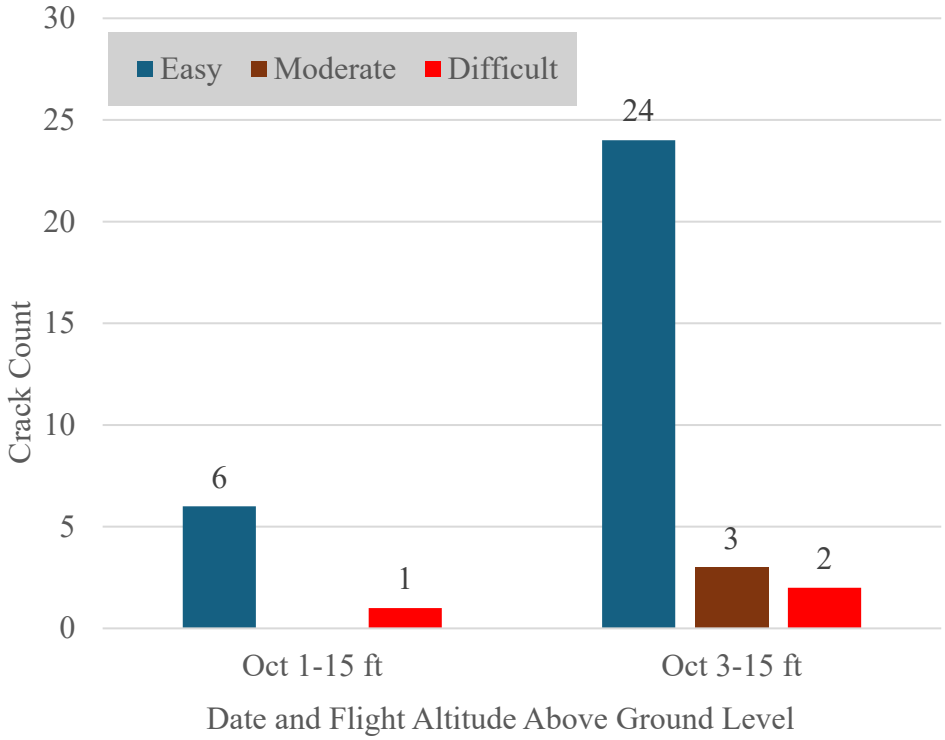

Figure 27. Visible cracks level of detection

Figure 28 illustrates the visibility counts across the four image classes, as first categorized in Figure 23. Even though the total number of images in each image class varies, one can generalize that the hairline cracks are visible across different classes. Since there was only one image classified as rough-shadow, it is premature to include that class under the stated generalization. Further comparison at the image classification level and the associated crack widths are shown in Figure 29 through Figure 32, with the conclusions summarized for each figure.

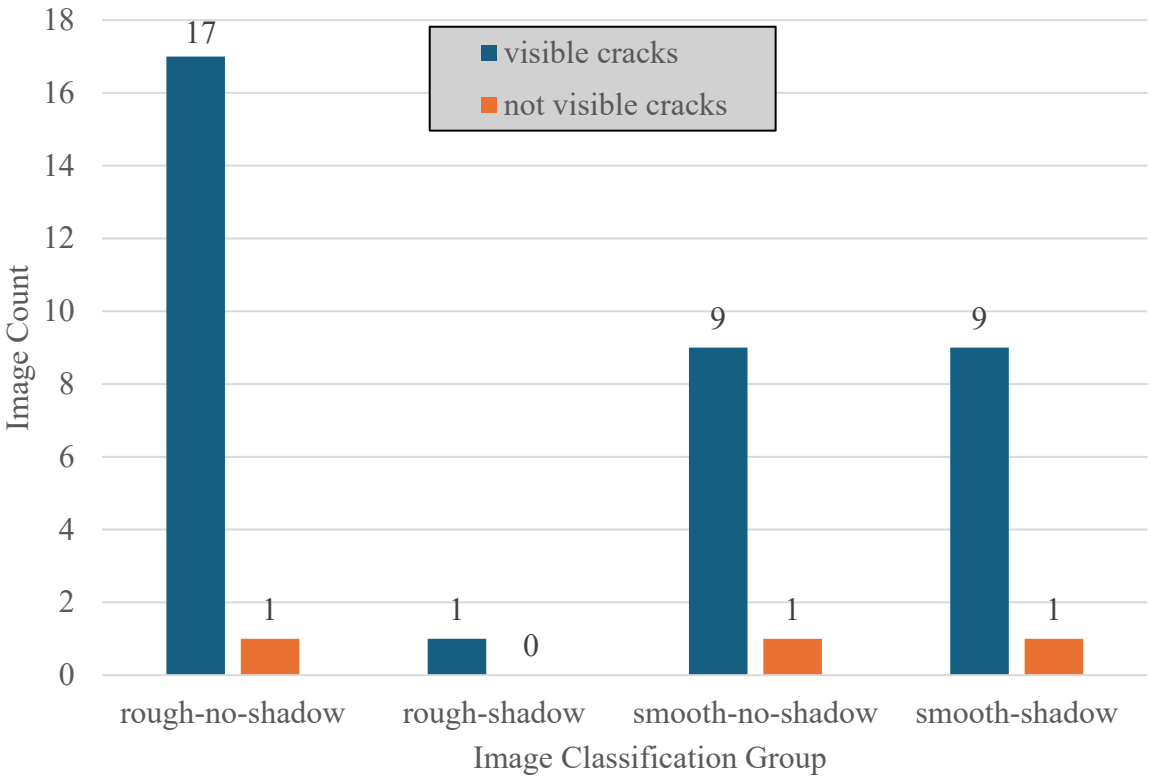

Figure 28. Visibility counts across combined image clusters for 15 ft (4.6 m) AGL data

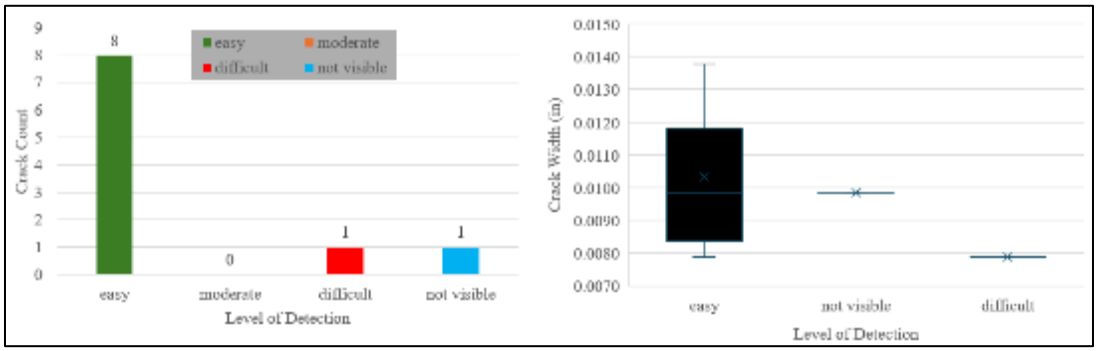

Figure 29. Level of detection counts (left) and detection category box plot (right) for smooth-shadow images, with the majority of cracks classified as easy and the level of detection decreasing with crack width

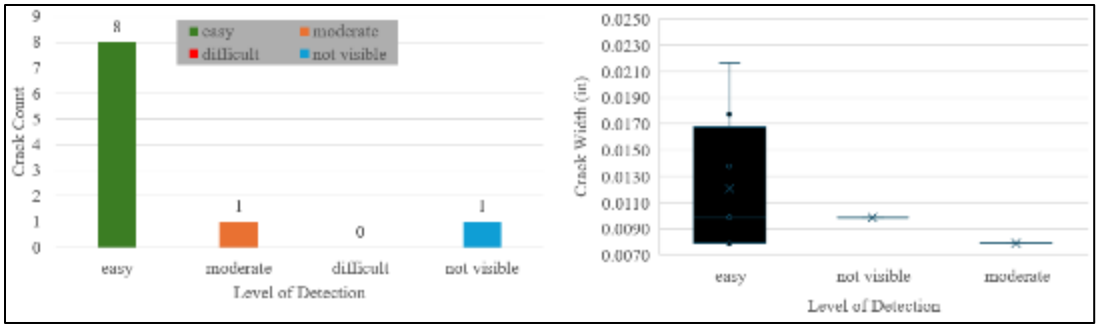

Figure 30. Level of detection counts (left) and detection category box plot (right) for smooth-no-shadow images, with the majority of cracks classified as easy and the level of detection decreasing with crack widths

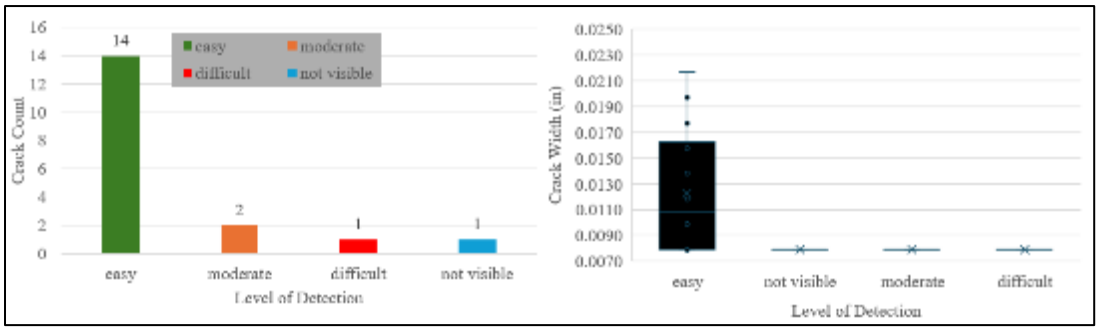

Figure 31. Level of detection counts (left) and detection category box plot (right) for rough-no-shadow images, with the majority of cracks classified as easy and an increase in the number of non-easy detections

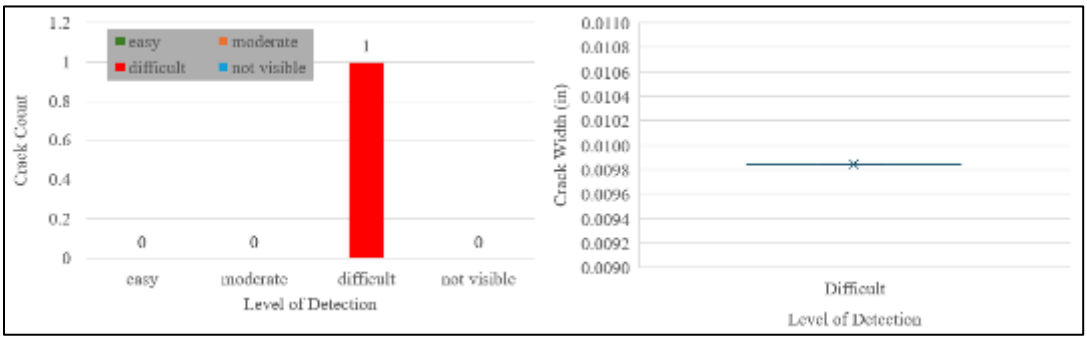

Figure 32. Level of detection counts (left) and detection category box plot (right) for rough-shadow images, with insufficient data for conclusions

Sample images cropped from the 15 ft (4.6 m) AGL orthophotos are shown in Figure 33 through Figure 38, with the images on the left side of each figure showing a marked hairline region at a scale of 1:30 and the images on the right side of each figure showing a zoomed-in section of each region at a scale of 1:5.

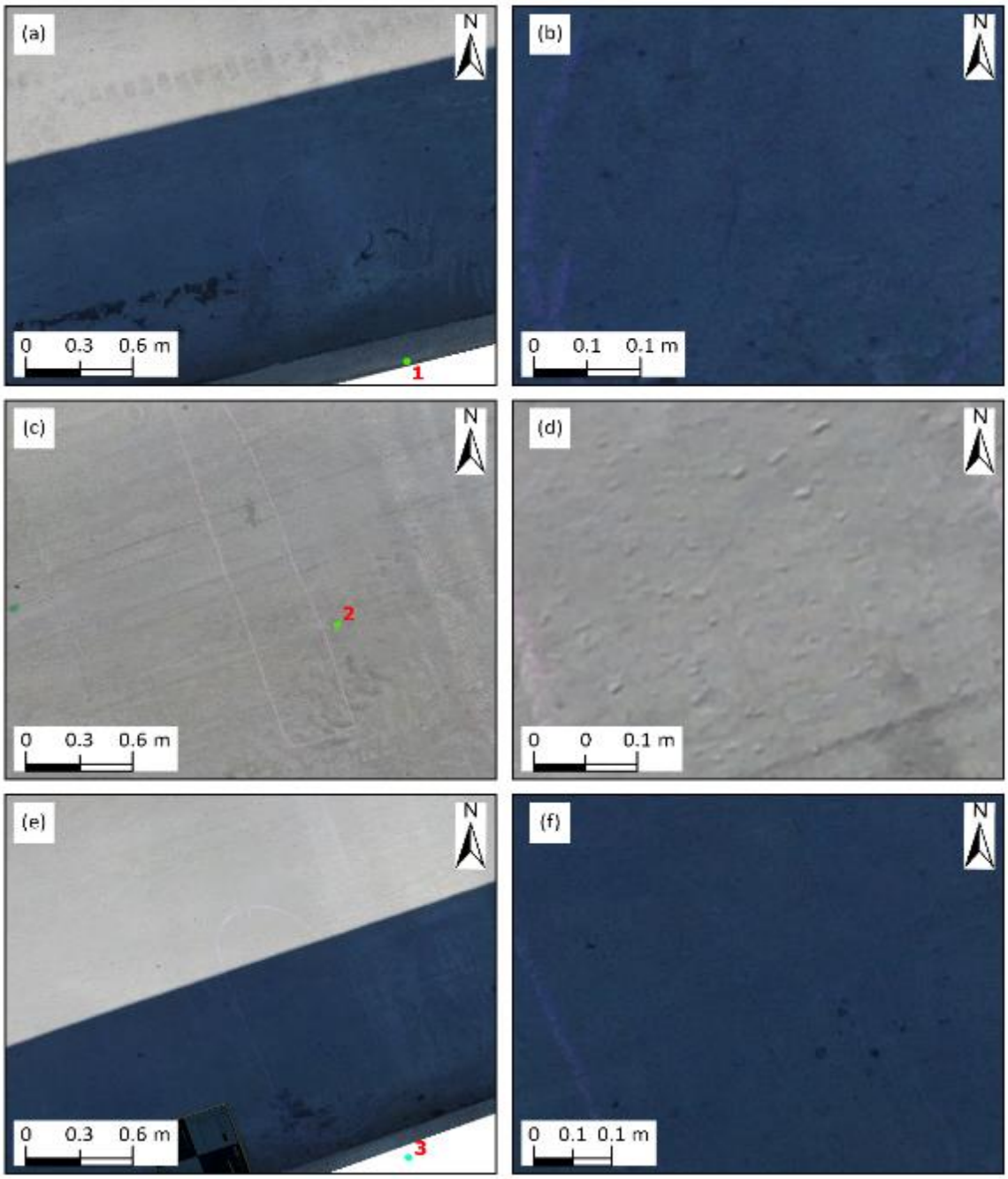

Figure 33. Cracks 1 through 3 at 0.032 in. (0.81 mm) GSD (1:30 zoom level on left and 1:5 zoom level on right)

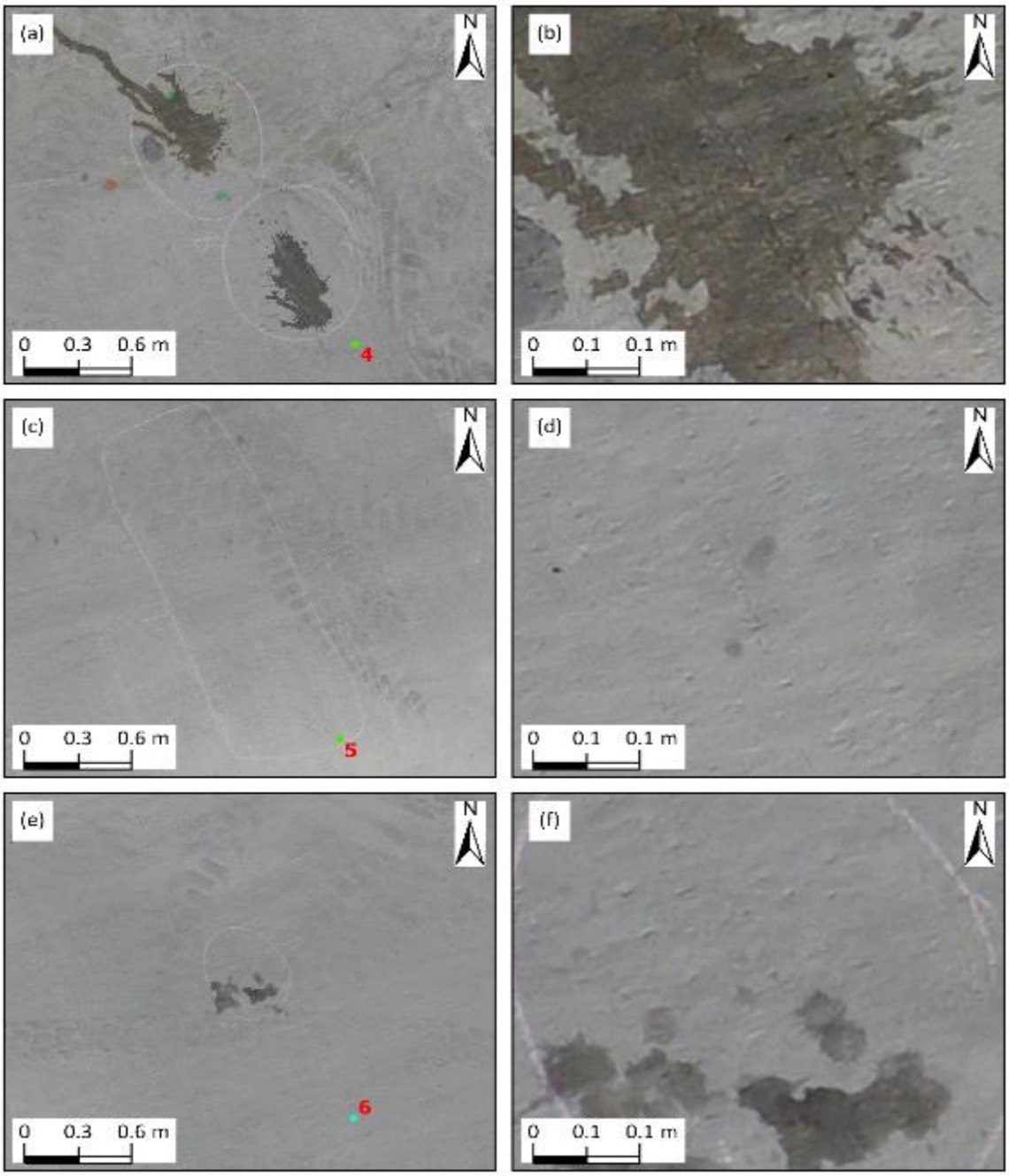

Figure 34. Cracks 4 through 6 at 0.032 in. (0.81 mm) GSD (1:30 zoom level on left and 1:5 zoom level on right)

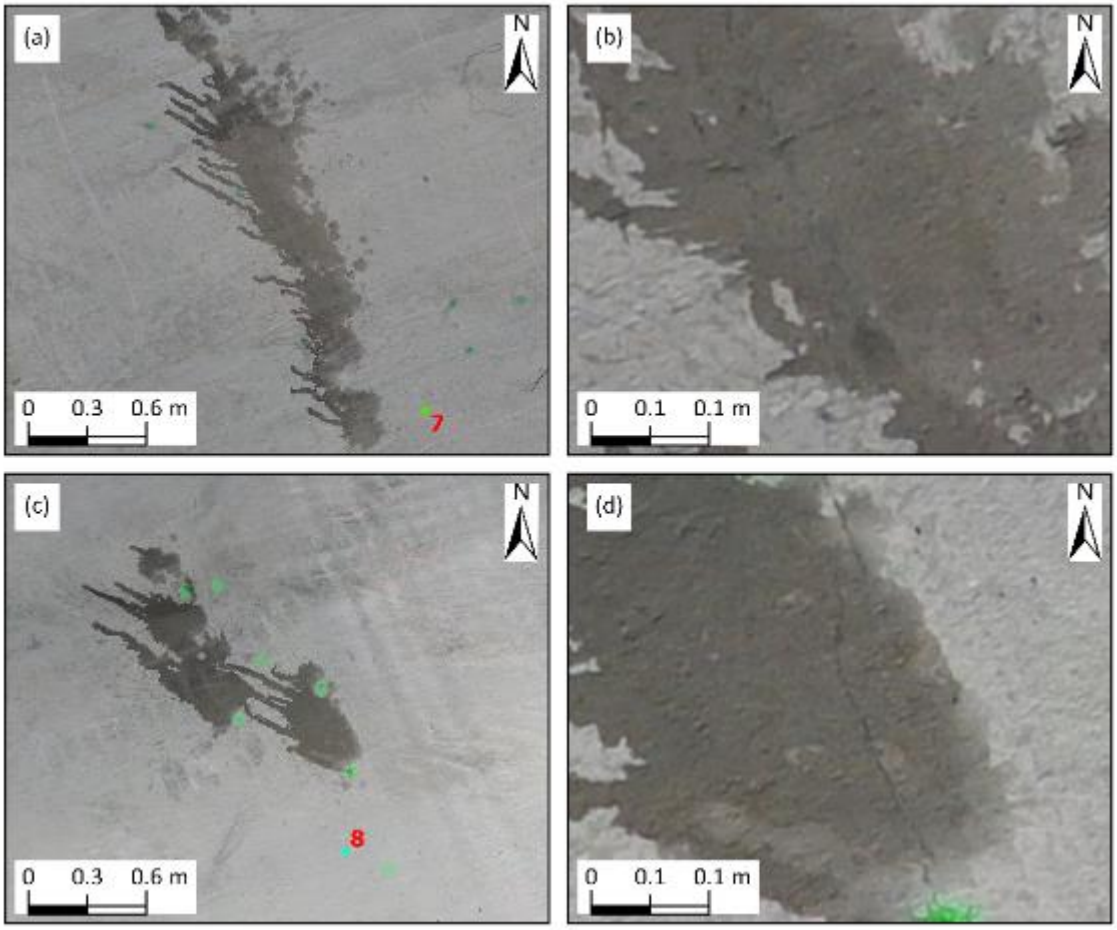

Figure 35. Cracks 7 and 8 at 0.032 in. (0.81 mm) GSD (1:30 zoom level on left and 1:5 zoom level on right)

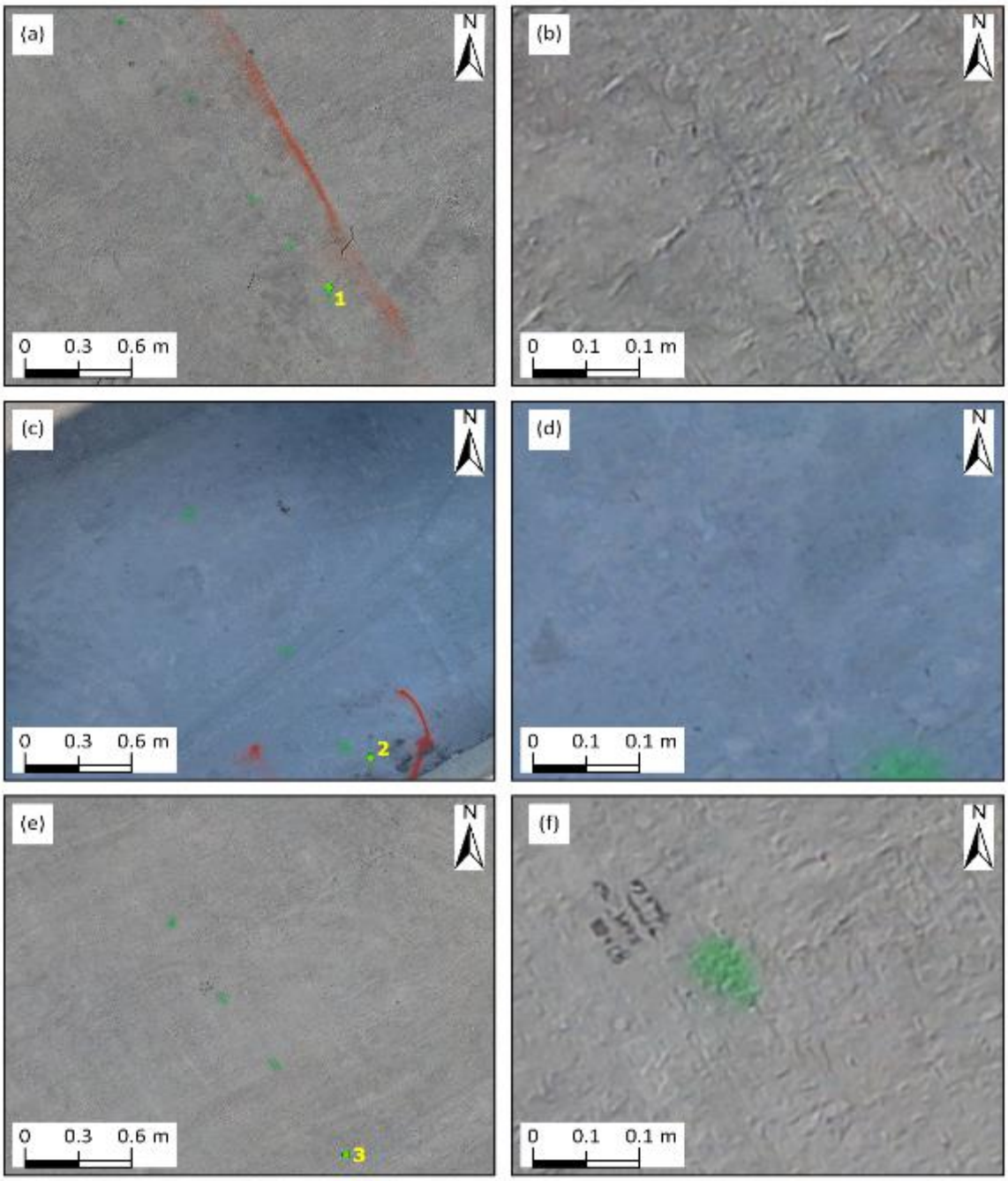

Figure 36. Cracks 1 through 3 at 0.035 in. (0.88 mm) GSD (1:30 zoom level on left and 1:5 zoom level on right)

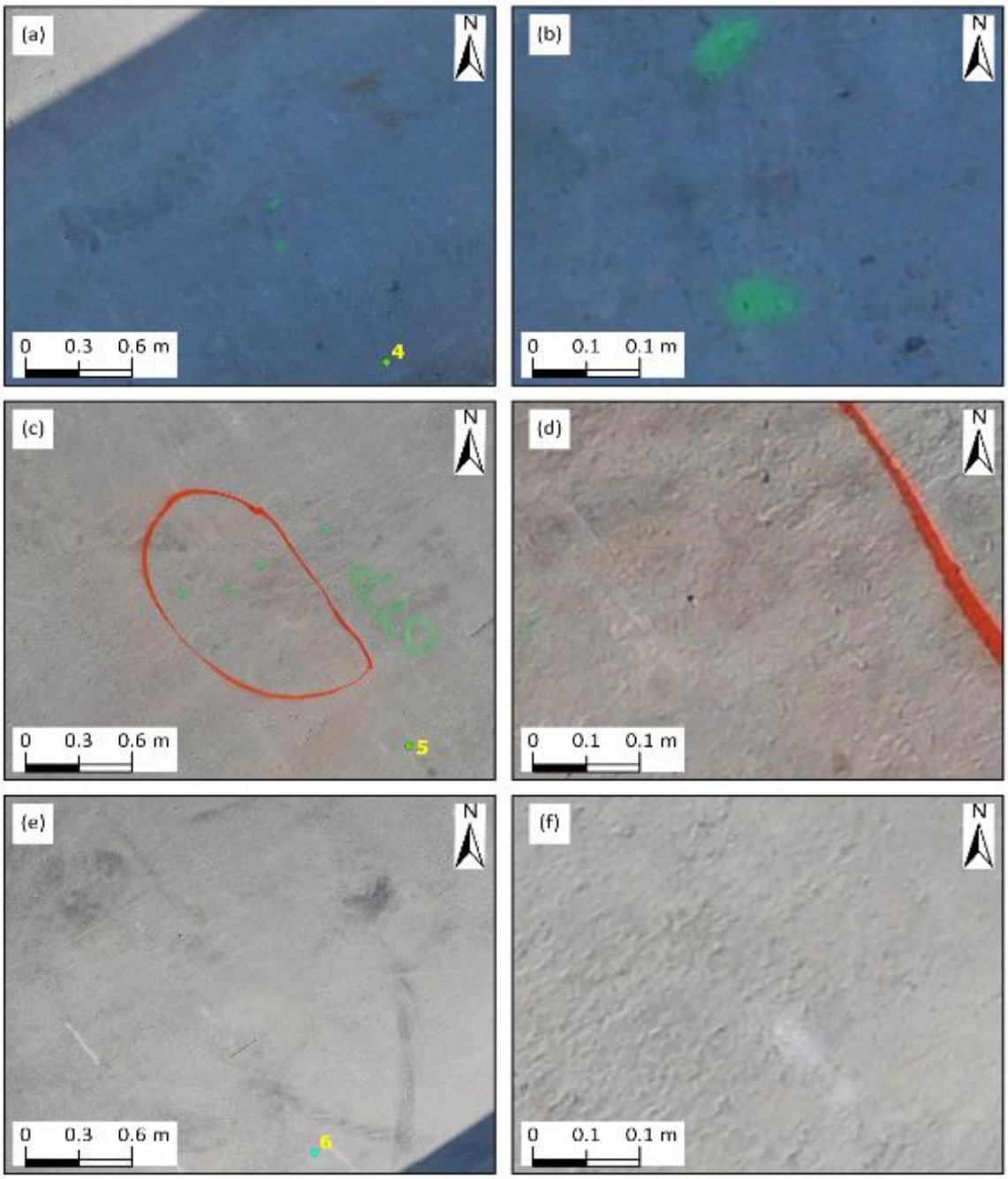

Figure 37. Cracks 4 through 6 at 0.035 in. (0.88 mm) GSD (1:30 zoom level on left and 1:5 zoom level on right)

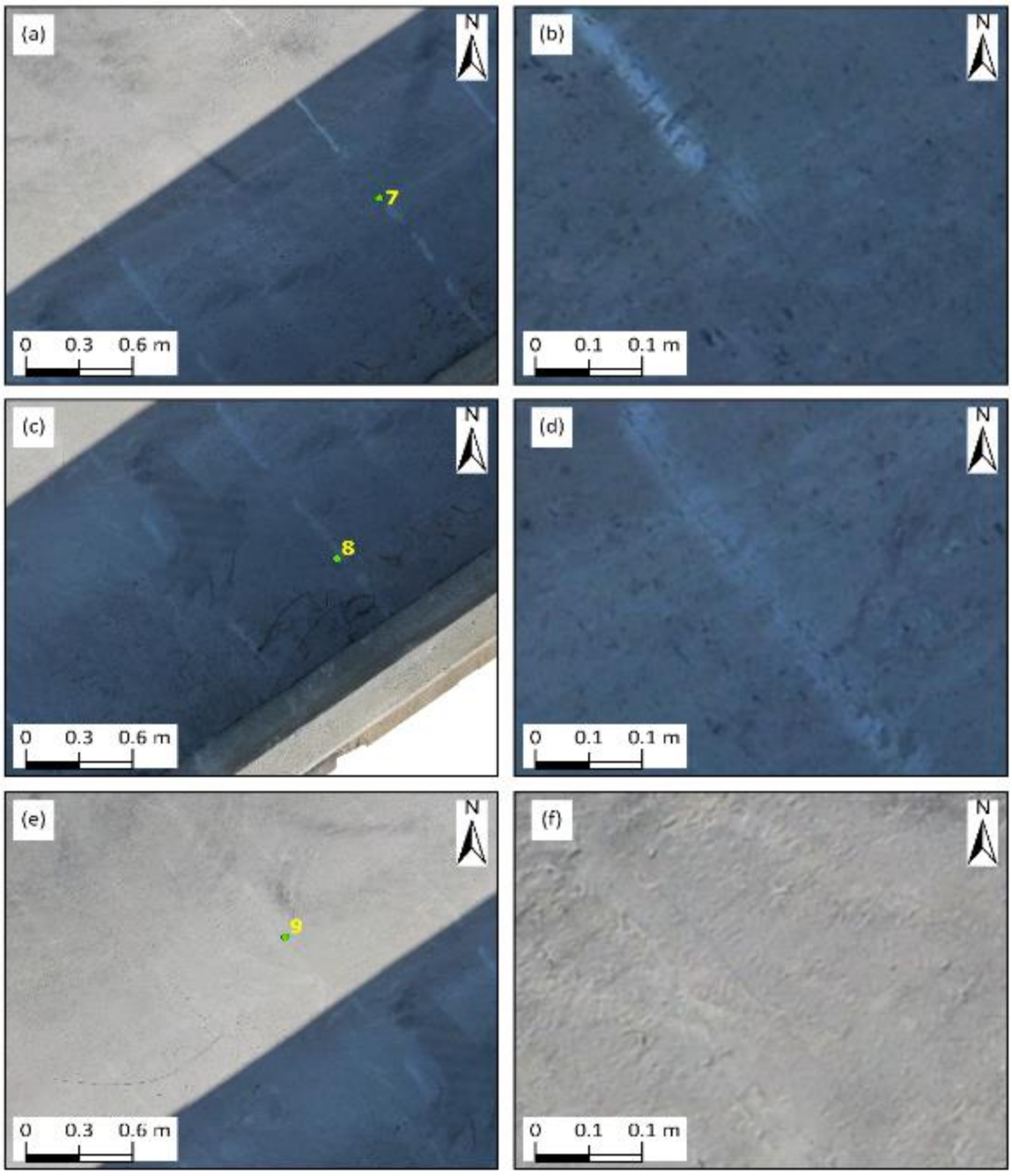

Figure 38. Cracks 7 through 9 at 0.035 in. (0.88 mm) GSD (1:30 zoom level on left and 1:5 zoom level on right)

Sample images cropped from the 35 ft AGL orthophotos are shown in Figure 39 and Figure 40, with the left side of each figure showing a marked hairline region at a scale of 1:20 and the right side of each figure showing a zoomed-in section of each region at a scale of 1:7.

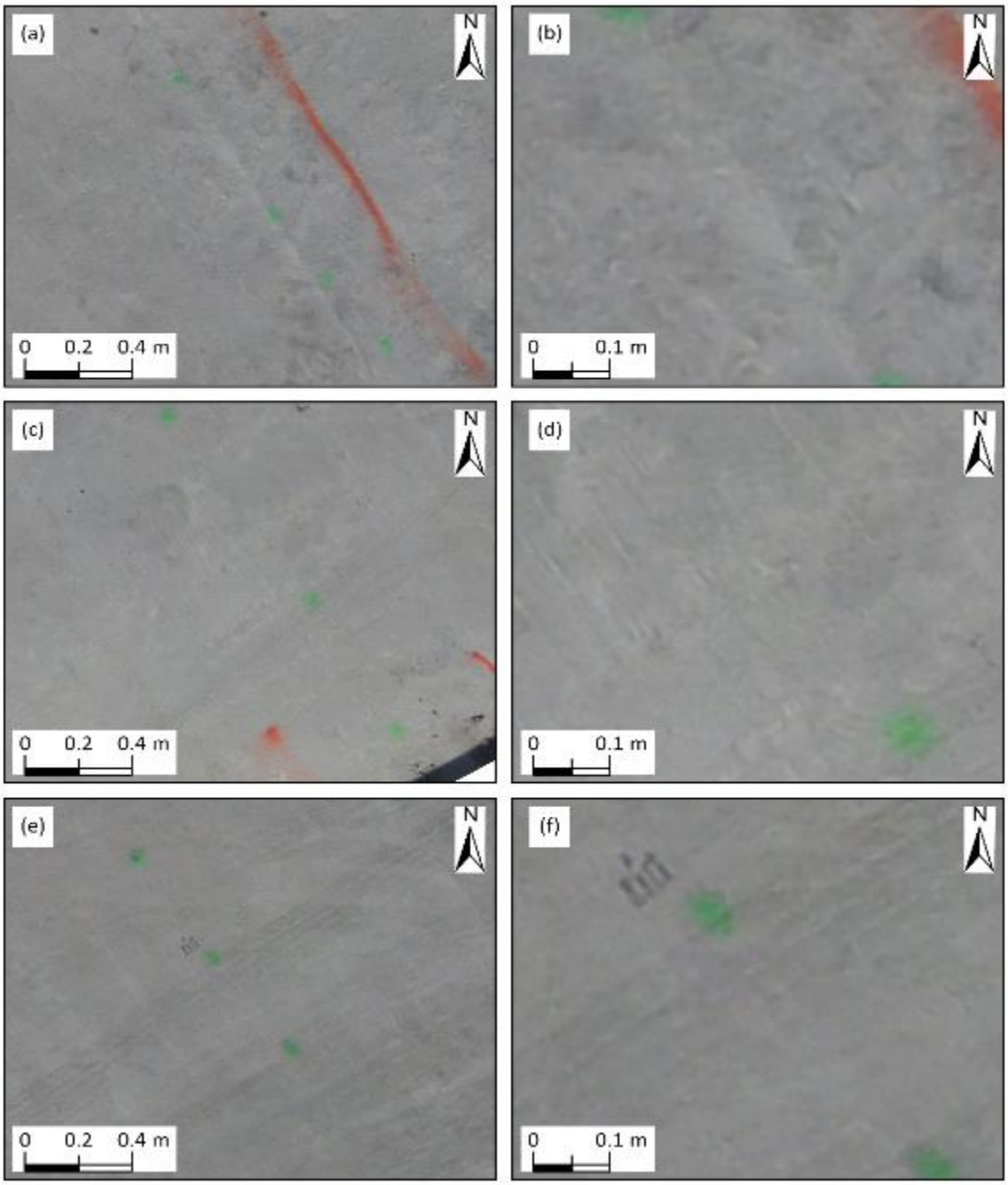

Figure 39. Cracks 1 through 3 at 0.066 in. (1.67 mm) GSD (1:20 zoom level on left and 1:7 zoom level on right)

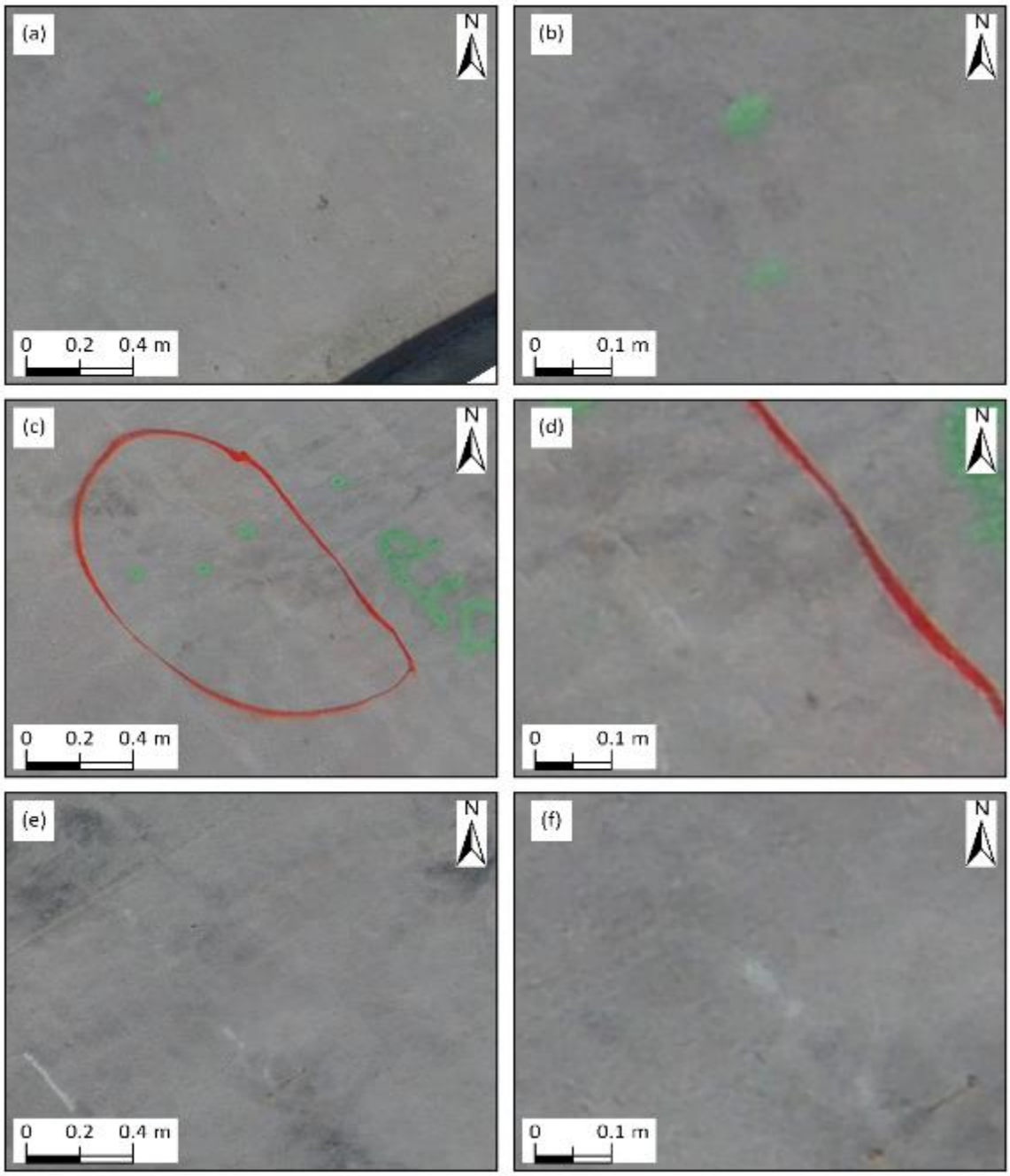

Figure 40. Cracks 4 through 6 at 0.066 in. (1.67 mm) GSD (1:20 zoom level on left and 1:7 zoom level on right)

3. HUMBOLDT COUNTY BRIDGE INSPECTION

On October 6, 2024, Cedric Wilkinson, representing the Iowa DOT, contacted the research team to explore the potential use of sUAS technology for inspecting cracks on a grooved concrete bridge in Humboldt County, Iowa (shown in Figure 41). The one-year-old bridge is 150 ft by 44 ft (45.7 m x 13.4 m), with crack widths ranging from hairline to more than 0.025 in. (0.635 mm). Unlike the NEMM bridge, which has a relatively steeper transverse and longitudinal slope, the Humboldt County bridge is nearly flat in the longitudinal direction and features approximately 2% cross slopes on either side of the centerline.

Figure 41. Satellite view image showing Humboldt County bridge bounded in red box

3.1. Objective

The objective of this data collection effort was to evaluate the effectiveness of high-resolution sUAS data collected at low altitudes for bridge deck hairline crack detection.

3.2. Field Data Collection

The research team developed a detailed data collection and safety plan a few days before going into the field. Availability was confirmed, and the necessary safety measures for an effective and safe data collection were discussed. On October 10, 2024, the research team, in collaboration with Iowa DOT personnel, conducted data collection at the Humboldt County bridge site. The research team followed safety guidelines to ensure efficient traffic flow and data collection. Before starting operations, the team conducted a safety briefing to ensure that all members were aware of potential hazards and emergency action plans. At first, traffic signs and cones were used to keep one lane open for vehicles (Figure 42). During this time, the team carried out a physical inspection of the bridge that focused on identifying and marking both hairline and significant cracks for measurement. Figure 43 shows the research team measuring and marking identified cracks on the bridge deck, while Figure 44 highlights examples of observed cracks.

The traffic management by Iowa DOT staff was critical for controlling traffic access during both automated and manual low-altitude flight operations.

Figure 42. Traffic control signs at both ends of the lanes

Figure 43. Research team manually inspecting the bridge and marking identified cracks

Figure 44. Identified and marked cracks on the bridge deck

While the longitudinally grooved bridge deck presented a challenge in distinguishing cracks from the grooved surface, particularly when cracks were aligned parallel to the grooves, transverse and angled cracks were easier to detect. After completing crack sampling and positioning six AeroPoints, full-lane closure was arranged and cones were removed from the median line to prepare for the first automatic mission flight at 40 ft AGL. Since the bridge is located outside controlled airspace, no flight approval was required. Figure 45 captures the flight in progress, which followed a longitudinal flight path with side and front overlaps ranging from 70% to 80%. Figure 45 illustrates the automatic flight path at a 40 ft altitude.

Figure 45. sUAS in automatic flight mode at 40 ft (12.2 m) AGL

The research team completed the 40 ft AGL flight in four minutes, and traffic flow resumed in one of the two lanes. Over the closed lane, the research team manually flew the sUAS at an altitude of 15 ft AGL, ensuring necessary overlap while following a longitudinal flight path similar to that of the automatic mission. Figure 46 illustrates the 15 ft manual flight path, and Figure 47 shows the remote pilot, a zoomed-in image of the sUAS in the air, and a passing vehicle in the open lane.

Figure 46. Manual mission flight at 15 ft (4.6 m) AGL

Figure 47. Manually controlled sUAS flight over a closed lane

After completing the first manual flight, all traffic was halted to transition to the other lane. Cones were repositioned to safeguard the laid AeroPoints, and the manual longitudinal flights were repeated at 15 ft AGL on the newly closed lane. Additional coverage was ensured by flying close to the mid-line section to achieve adequate overlap. Following data collection from both lanes, the research team ordered a full lane closure, removing all cones and AeroPoints from the bridge to conclude the operation.

3.3. Data Processing

The data collected from the Humboldt County bridge were processed in two sets. A computer equipped with an Intel Xeon W-2265 processor (19.25M cache, 3.50 GHz) with 12 cores and 24 threads, 128 GB DDR4 ECC RAM, and a NVIDIA QUADRO RTX 5000 16 GB graphic card with 3,072 CUDA cores was used for this processing. The sUAS data were processed in two batches: data collected at 40 ft (12.2 m) AGL and data collected at 15 ft (4.6 m) AGL. The research team used six AeroPoints during the data collection, but only five AeroPoints recorded the data processed and used to correct image location information. The same data collection workflow used for the NEMM bridge data processing was used for the Humboldt County bridge data processing; the data processing times, steps, and resolution information are shown in Table 4. Snapshots of the orthophotos are provided in Figure 48 and Figure 49.

Table 4. Data collection and processing details

Section	Images	Capture Time (mins)	Time Required (mins)					GSD (in. (mm))
			Alignment	Depth Maps	Model	Ortho	Total	
15 ft	789	45	39	340	137	136	652	0.033 (0.85)
40 ft	79	4	3	30	30	25	88	0.079 (2.02)

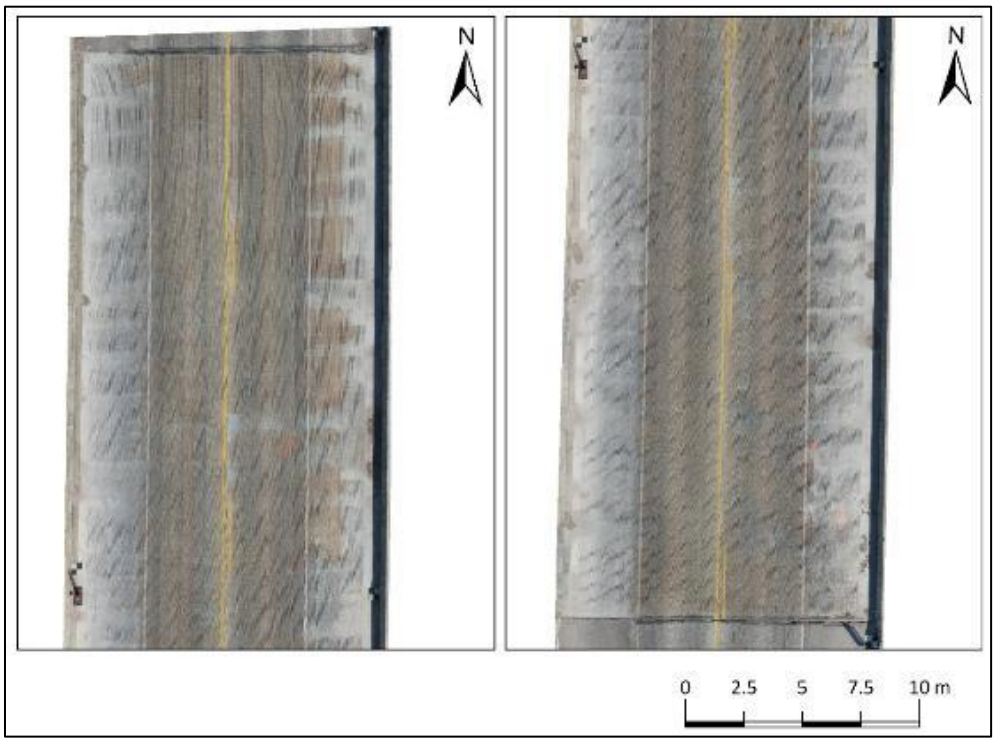

Figure 48. Processed orthophotos from sUAS data collected at 15 ft (4.6 m) AGL

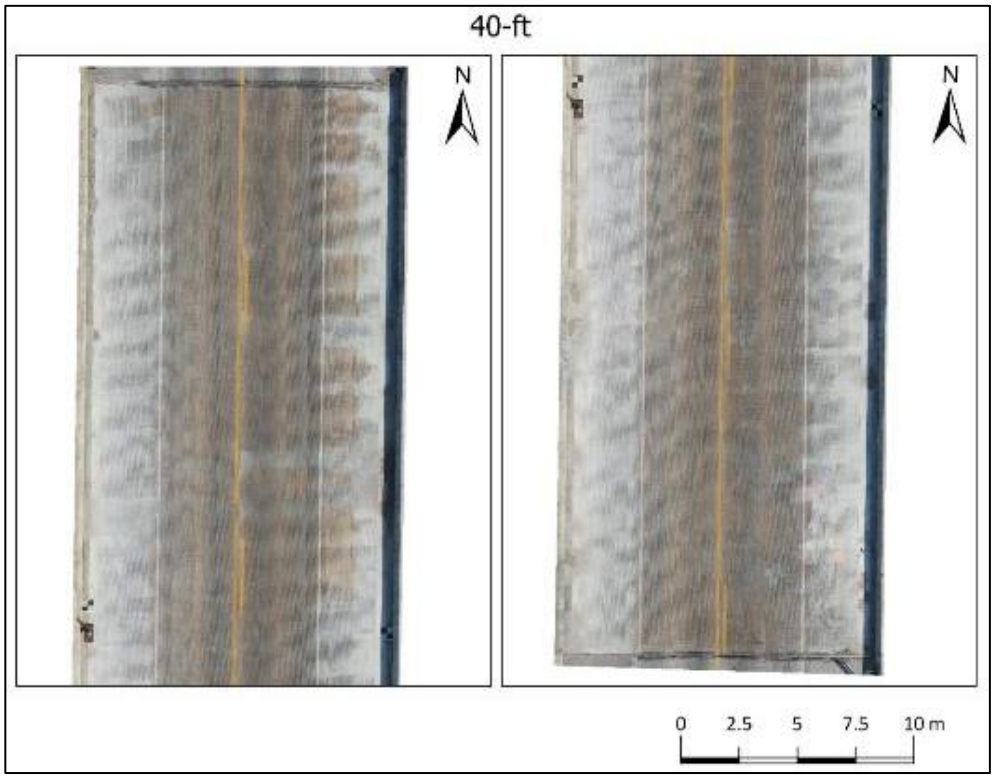

Figure 49. Processed orthophotos from sUAS data collected at 40 ft (12.2 m) AGL

3.4. Data Analysis

During a quick manual inspection of one of the bridge lanes, the research team identified and measured nine cracks. As shown in Figure 50, the crack widths ranged from 0.0138 to 0.0295 in (0.351 to 0.749 mm). Sample images of these cracks captured at 15 ft (4.6 m) and 40 ft (12.2 m) AGL are presented in Figure 51 through Figure 56. Visibility analysis of the cracks was conducted using a methodology similar to that used for the NEMM bridge. Only orthoimages at a baseline scale of 1:4 for the 15 ft (4.6 m) AGL flight were shared with reviewers to assess the level of detection, using a template similar to the one used for the NEMM bridge. Table 5 shows the reviewers' label count and final score for the 15 ft (4.6 m) AGL data using a scoring weight and defuzzification range similar to the one described in Section 3.6. However, the research team mainly focused on the 15 ft (4.6 m) AGL data since the poor resolution in the 40 ft (12.2 m) AGL images resulted in the determination of no visible cracks.

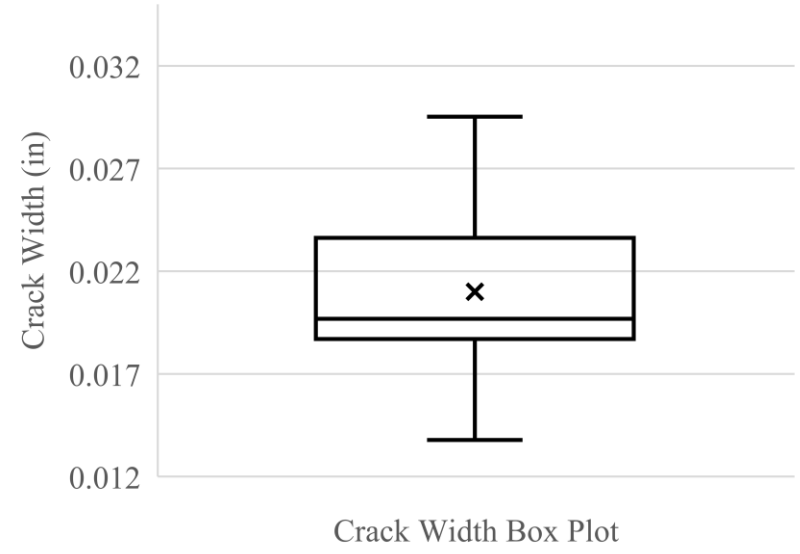

Figure 50. Boxplot of measured crack widths

Table 5. Aggregated reviews and final score for 15 ft (4.6 m) data

Crack ID	Easy	Moderate	Difficult	Not Visible	Final
1	0	1	3	1	difficult
2	2	1	2	0	moderate
3	0	0	3	2	not visible
4	0	2	2	1	difficult
5	0	1	1	3	not visible
6	0	0	1	4	not visible
7	0	1	2	2	not visible
8	5	0	0	0	easy
9	5	0	0	0	easy

As shown in Table 5 , six of the nine identified cracks were generally visible, though of varying difficulty to detect. In summary, distinguishing between cracks and the grooved surface of the bridge deck was challenging even though the crack widths were, on average, wider than the crack widths on the NEMM bridge. The last two crack samples, 8 and 9, were generally easy to detect because they were located outside the grooved lanes, thus providing better contrast that aided visibility.

Sample images cropped from the 40 ft (12.2 m) AGL orthophotos are shown in Figure 51 through Figure 53, with the left side of each figure showing a marked hairline region at a scale of 1:20 and the right side of each figure showing a zoomed-in section of each region at a scale of 1:7.

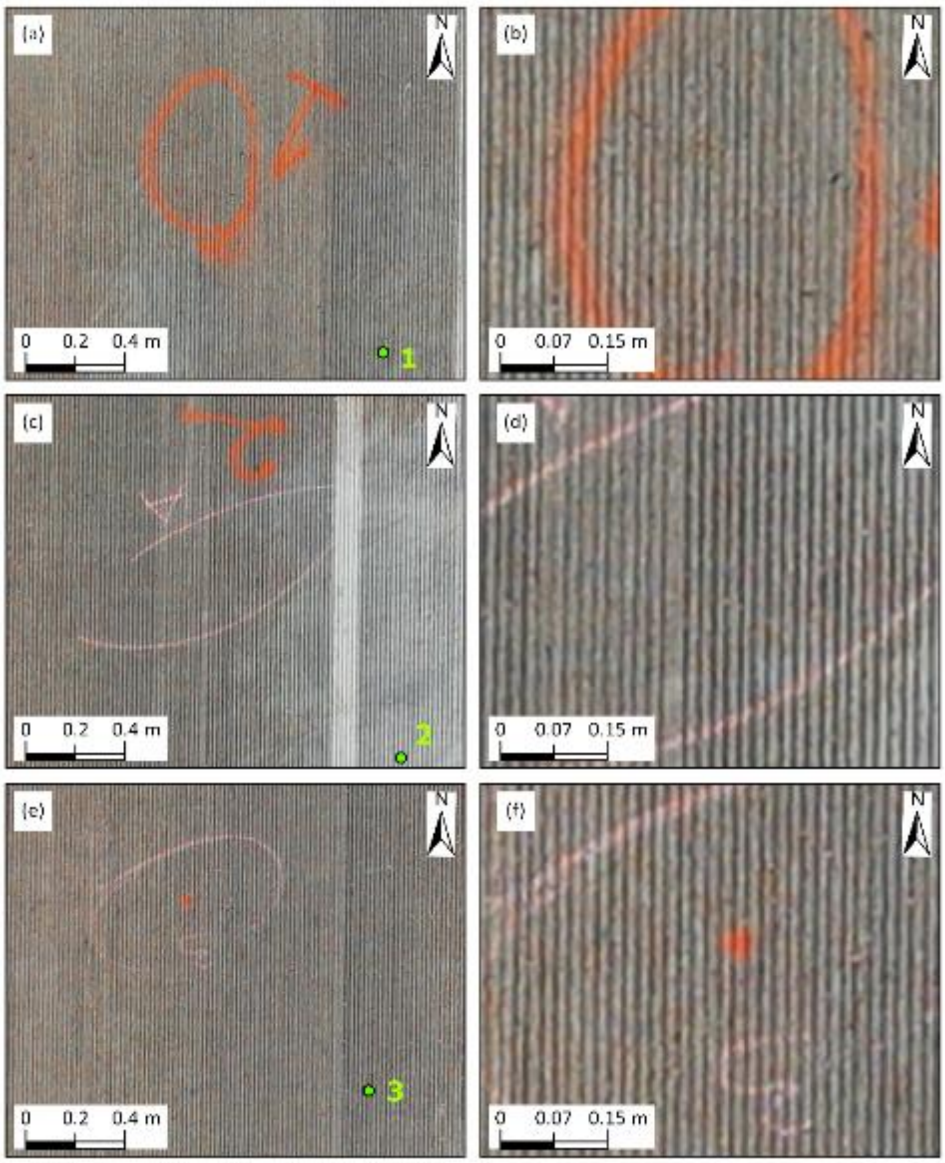

Figure 51. Cracks 1 through 3 at 0.079 in. (2.02 mm) GSD (1:20 zoom level on left and 1:7 zoom level on right)

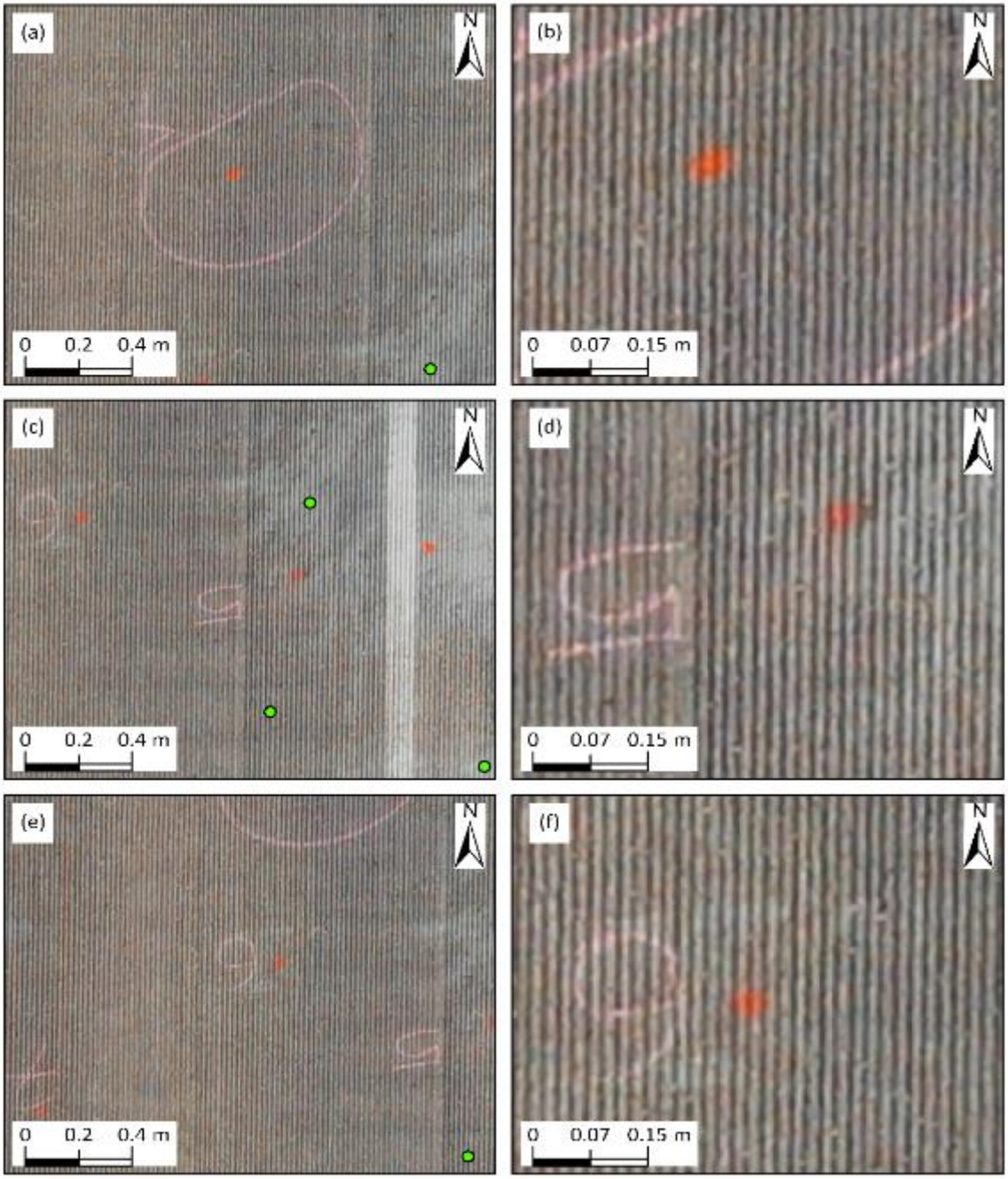

Figure 52. Cracks 4 through 6 at 0.079 in. (2.02 mm) GSD (1:20 zoom level on left and 1:7 zoom level on right)

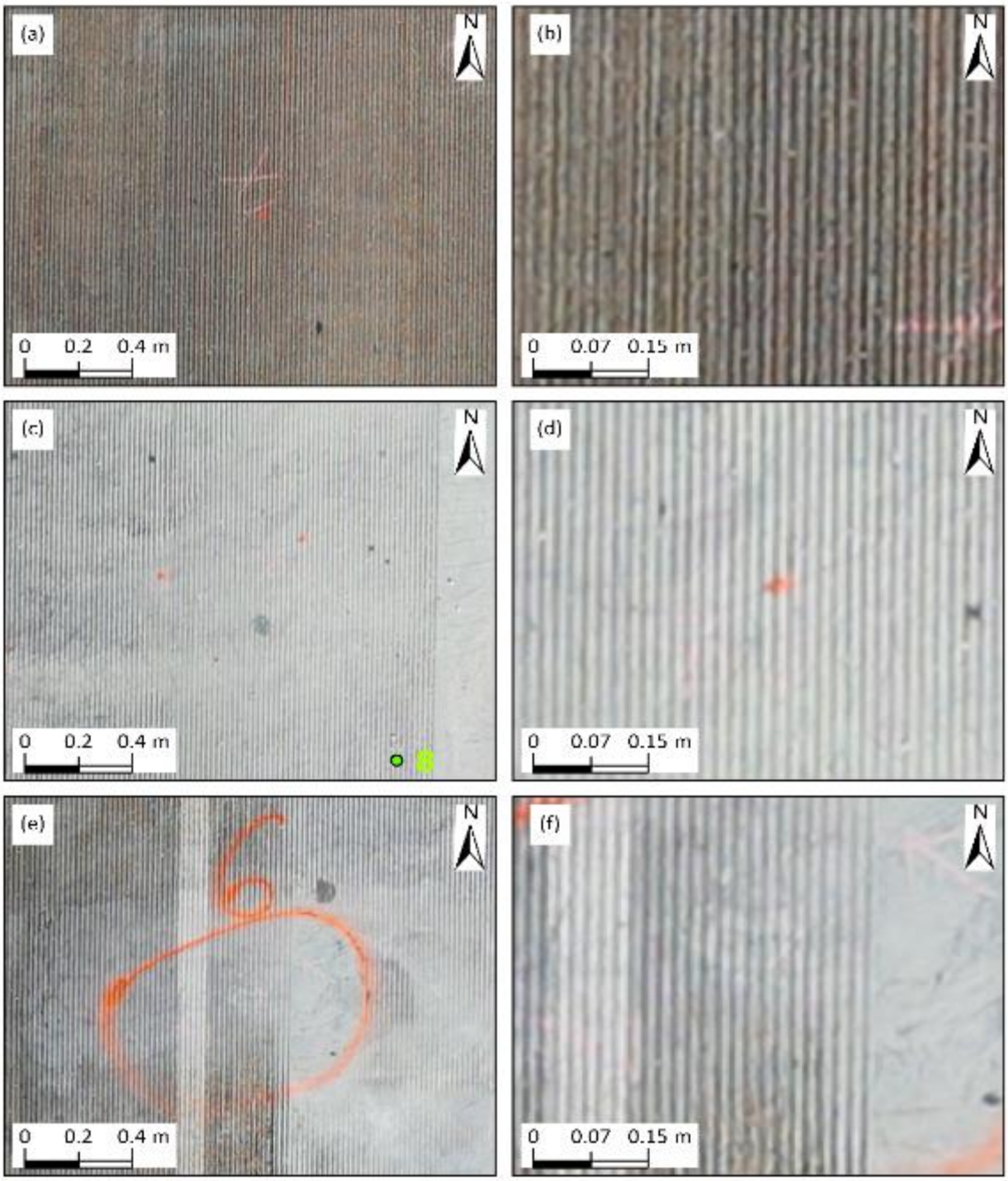

Figure 53. Cracks 7 through 9 at 0.079 in. (2.02 mm) GSD (1:20 zoom level on left and 1:7 zoom level on right)

Sample images cropped from the 15 ft (4.6 m) AGL orthophotos are shown in Figure 54 through Figure 56, with the left side of each figure showing a marked hairline region at a scale of 1:20 and the right side of each figure showing a zoomed-in section of each region at a scale of 1:6.

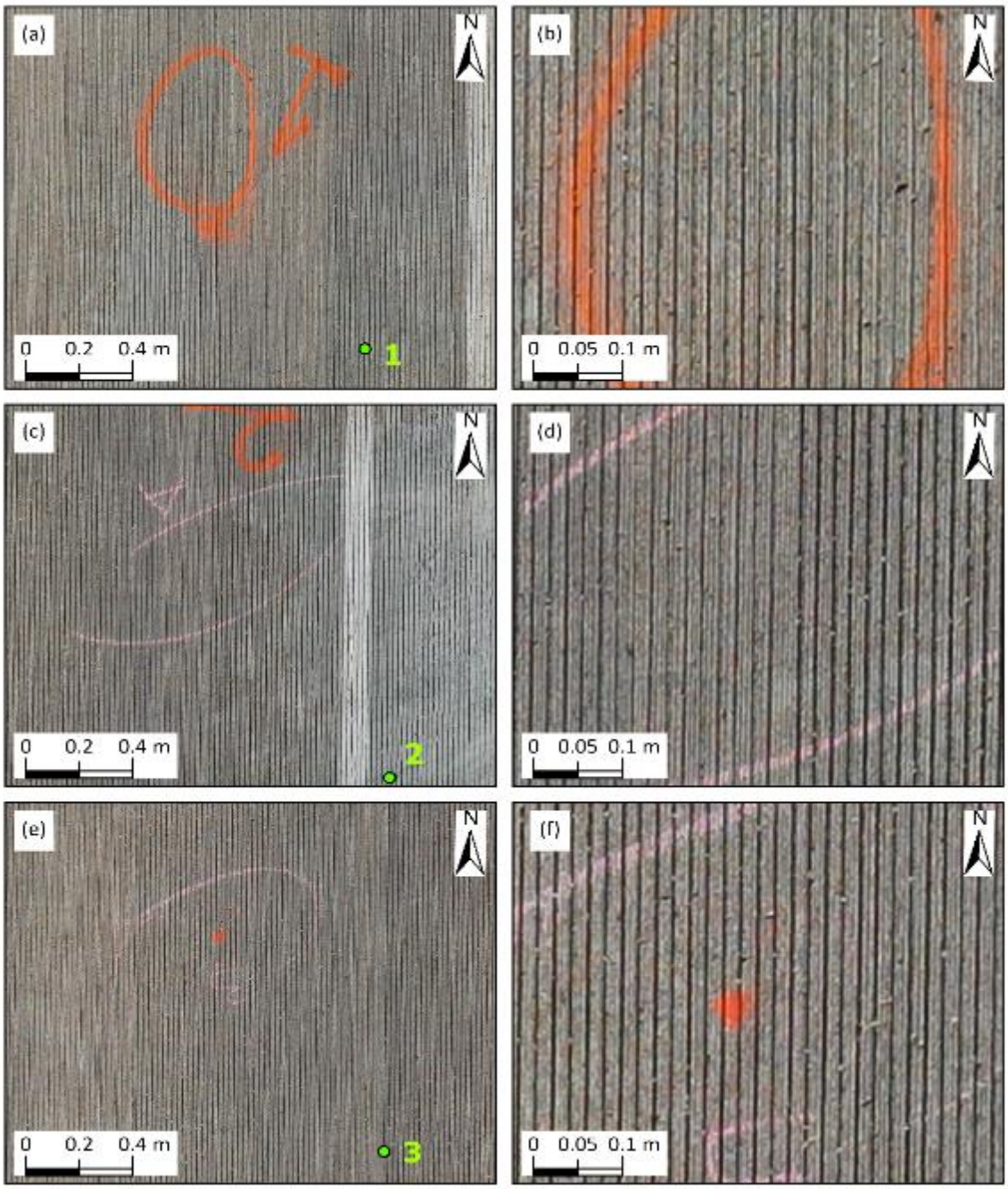

Figure 54. Cracks 1 through 3 at 0.033 in. (0.85 mm) GSD (1:20 zoom level on left and 1:6 zoom level on right)

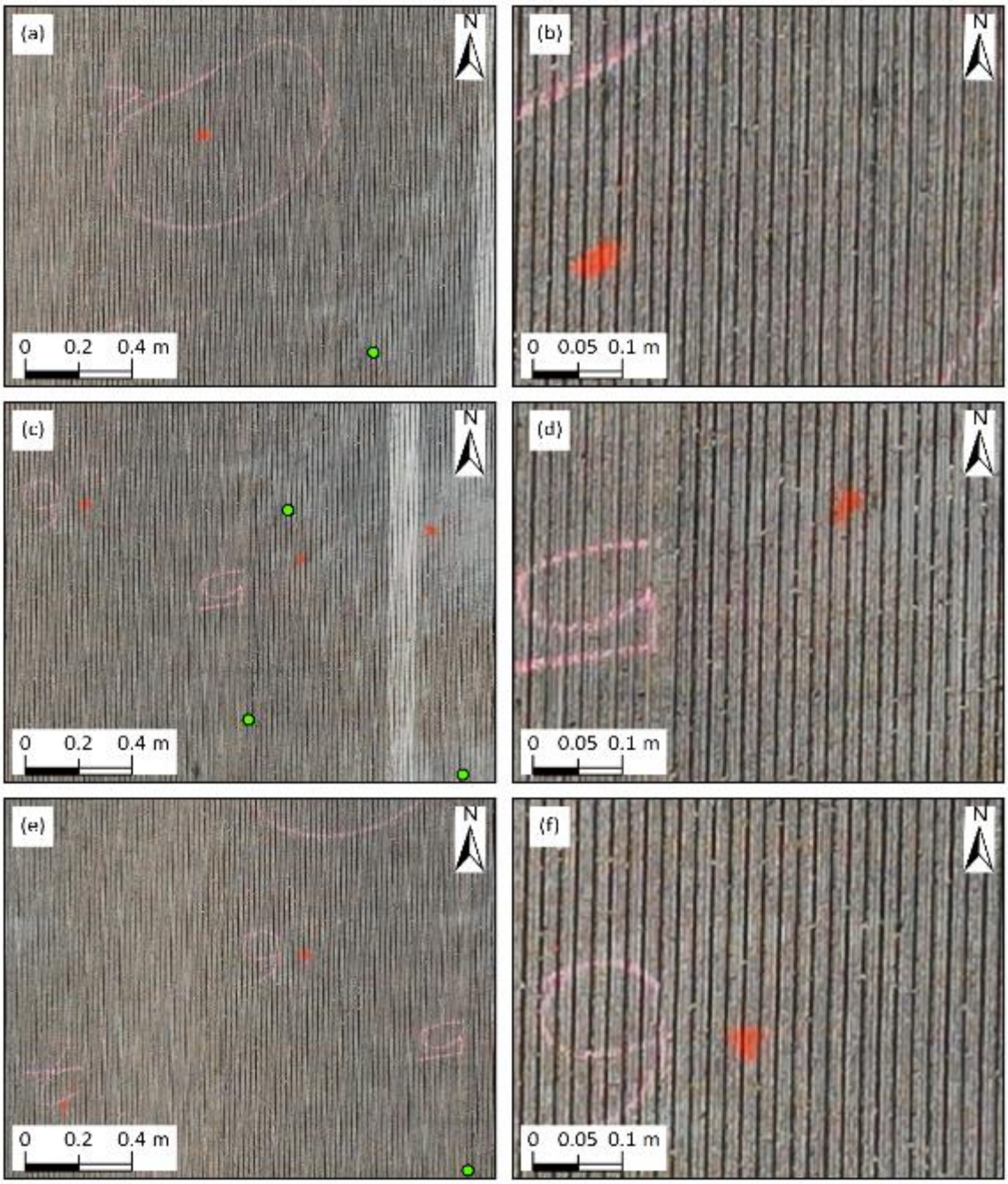

Figure 55. Cracks 4 through 6 at 0.033 in. (0.85 mm) GSD (1:20 zoom level on left and 1:6 zoom level on right)

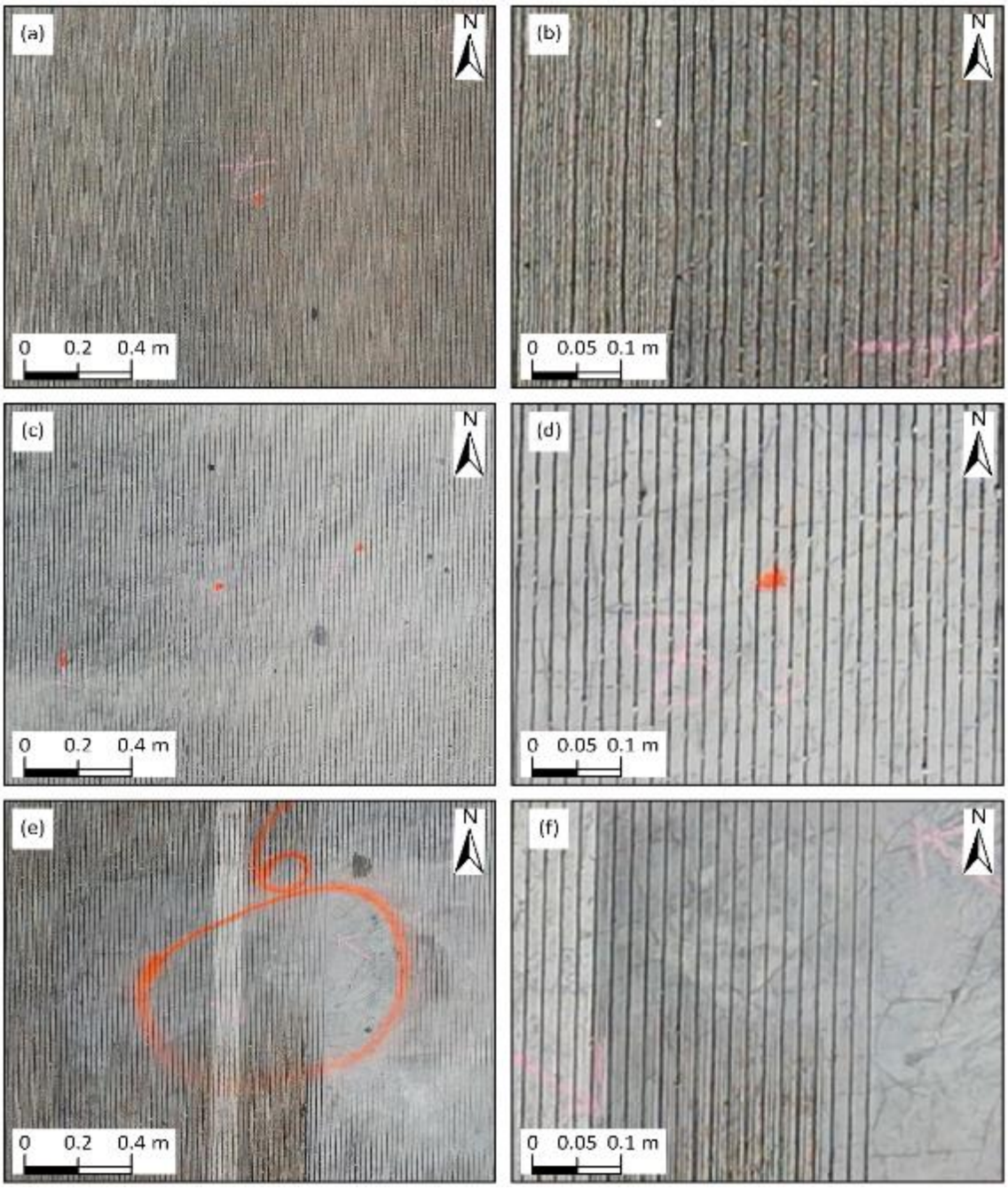

Figure 56. Cracks 7 through 9 at 0.033 in. (0.85 mm) GSD (1:20 zoom level on left and 1:6 zoom level on right)

4. LESSONS LEARNED AND RECOMMENDATIONS

4.1. NEMM Bridge: Lessons Learned and Recommendations

The research team visited the NEMM bridge site on three occasions and collected sUAS data at two different altitudes. The lessons learned during the data collection, processing, and analysis are presented below.

4.1.1. Lessons Learned

- Low-altitude flights at 15 ft (4.6 m) AGL could only be flown manually, and therefore data collection took a relatively long time. For example, it took a total of 225 minutes of flight time to cover the NEMM Unit 1 section, while the same coverage would typically have been achieved in 25 minutes if the sUAS had been flown automatically at 50 ft (15.2 m) AGL. Such prolonged manual data collection led to uneven shadow patterns on the bridge deck as shadows shifted over time.
- Since manual flight is hard to control and prone to inconsistencies in speed and overlap, the PIC was cautious to ensure that the sUAS remained on the preplanned route and avoided flying directly above passing vehicles.
- The relatively steep longitudinal slope of the bridge deck required adjustments to the sUAS's altitude mid-flight to maintain a consistent image resolution, and this was difficult. The flight altitude from the pavement had slight variations.
- An average wind gust of 13 mph (5.8 m/s) posed significant safety concerns during manual flights, causing the suspension of data collection on the second day of sUAS inspection.
- Passing trucks on the bridge deck required the team to remain vigilant. The VO actively monitored and communicated with the pilot and truck drivers throughout the operation. The presence of parked heavy-duty equipment under the bridge also limited the drone's ability to collect additional underdeck data.

4.1.2. Recommendations

- Achieving sub-millimeter accuracy is crucial for detecting fine cracks from sUAS-collected images.
- To mitigate inconsistencies during manual flight, the flight mode was set to "Tripod," the speed was reduced to 1 to 2 mph, and bridge edges were marked at 6 to 7 ft (1.8 to 2.1 m) intervals to indicate transverse lines for each pass.
- Portable and smaller-sized sUAS such as the DJI Mavic Enterprise are more suitable and safer for low-altitude flights than bigger counterparts like the DJI Matrice 600 Pro.
- A 15 ft (4.6 m) AGL flight altitude is highly recommended when sufficient time and resources are available. To reduce data collection time without compromising data quality, it is recommended for follow-up demonstrations that a camera (e.g., LR1 or Nikon D850) with a higher resolution of 60 MP to 100 MP be deployed at higher altitudes.
- A minimum of three team members are required for three roles: (1) piloting, (2) visually observing the sUAS, and (3) providing logistical support for data collection.

- It is recommended that provisions for multiple flight sessions be made by ensuring that a power source is available for charging on-site.
- To avoid disruptions, conduct a detailed weather analysis before selecting inspection dates, and monitor the weather closely during flight periods.
- In the event of sudden weather changes that create unfavorable or unsafe flying conditions, suspend all flights immediately. Always prioritize safety.

4.2. Humboldt County Bridge: Lessons Learned and Recommendations

The research team visited the Humboldt County bridge site and collected sUAS data at two different altitudes (40 ft [12.2 m] and 15 ft [4.6 m]). The lessons learned during the data collection, processing, and analysis are presented below.

4.2.1. Lessons Learned

- Traffic management was crucial for achieving fast and efficient data collection on the busy bridge section. To minimize driver waiting times during manual flights, one lane was kept open to traffic while flights were conducted in the closed lane. The close proximity of the two lanes required the remote pilot to exercise extreme caution when operating near the mid-lane boundary line.
- The sight of the drone in the air attracted the attention of drivers, resulting in distracted driving.
- Even with low-altitude flights, remotely detecting cracks on the grooved deck surface from the orthophoto images proved challenging due to the texture and alignment of the grooves.
- Traffic disruptions were significantly mitigated thanks to the staff and traffic control equipment provided by the Iowa DOT. Managing traffic could potentially become a significant bottleneck without sufficient personnel support.

4.2.2. Recommendations

- The recommendations provided in Section 4.1.2 are also applicable to this data collection effort.
- The relatively larger crack widths reduced the difficulty of manually detecting cracks on the grooved surface, although longitudinal cracks were harder to detect due to their alignment with the groove orientation.
- Since it was difficult to detect grooved cracks from 15 ft (4.6 m) AGL images, at least with the M2EA 48 MP quad-bayer imaging sensor, higher-resolution data collection using more capable sUAS systems and cameras is recommended.

5. CONCLUSIONS

The research team collected high-resolution sUAS data from two bridges in Iowa to evaluate the efficacy of the sUAS in detecting hairline cracks. The M2EA sUAS, with its 48 MP RGB camera, was used for 15 ft (4.6 m) AGL and 35 ft (10.7 m) AGL data collection at the NEMM bridge. This resulted in GSDs of 0.026 in. (0.66 mm), 0.032 in. (0.81 mm), and 0.035 in. (0.88 mm) for three-part processing of the 15 ft (4.6 m) AGL data and a GSD of 0.066 in. (1.67 mm) for the 35 ft (10.7 m) data. The same sUAS was used for 15 ft (4.6 m) AGL and 40 ft (12.2 m) AGL data collection at the Humboldt County bridge, resulting in GSDs of 0.033 in. (0.85 mm) and 0.079 in. (2.02 mm). The research team marked and measured the widths of 39 cracks on the NEMM bridge and 9 cracks on the Humboldt County bridge and analyzed the efficacy of using RGB data for the remote sensing of hairline cracks.

The analysis showed that low-altitude flights (e.g., 15 ft [4.6 m] AGL) are critical for achieving the sub-millimeter accuracy necessary for detecting hairline cracks. The resulting aggregation from the crack analysis also showed that while high-resolution data derived from low-altitude flights aided in detecting hairline cracks on structures with ungrooved surfaces, it is challenging to utilize a similar framework for hairline cracks on structures with grooved surfaces. This assertion is supported by the final detection level from the ungrooved NEMM bridge, which had a total of 36 visible cracks out of 39 presented, 30 of which were rated as easy to detect. Approximately half of the cracks on the grooved Humboldt County bridge deck were not visible, as only the observable cracks found outside of the main lane—a high-contrast and lightly grooved area—were rated as relatively easy to detect.

The analysis also showed that the finer (narrower) the crack width, the more challenging its detection. The identified image classes in this study (smooth-shadow, smooth-no-shadow, rough-shadow, and rough-no-shadow) for the most part showed consistent results in terms of a high number of easy detections, except for the rough-shadow class. This latter class had only one image, and therefore it was considered premature to draw conclusions about this class.

Manual flight at low altitudes is labor-intensive, time-consuming, and prone to inconsistencies in speed and overlap. These drawbacks can be mitigated by using the “Tripod” mode on the drone, marking crosswise reference lines for proper overlap, and employing high-resolution cameras. Deployment of higher-resolution camera systems at a greater altitude to obtain better overlap and spend less time on data collection is likely a practical solution. External factors like wind gusts and steep slopes require careful planning and adaptive strategies.

In conclusion, this study provided practical insights into applying sUAS for infrastructure inspection. The lessons learned and recommendations from the two bridge case studies presented can guide future endeavors, ensuring efficient, accurate, and safe implementation of sUAS technology in transportation monitoring tasks.

REFERENCES

Aela, P., H.-L. Chi, A. Fares, T. Zayed, and M. Kim. 2024. UAV-based studies in railway infrastructure monitoring. *Automation in Construction*, Vol. 167.

Banić, M., A. Miltenović, M. Pavlović, and I. Ćirić. 2019. Intelligent machine vision based railway infrastructure inspection and monitoring using UAV. *Facta Universitatis, Series: Mechanical Engineering*, Vol. 17, No. 3, pp. 357–364.

BLS. 2019. Census of Fatal Occupational Injuries Summary. Bureau of Labor Statistics. https://www.bls.gov/news.release/cfoi.nr0.htm.

Escobar-Wolf, R., T. Oommen, C. N. Brooks, R. J. Dobson, and T. M. Ahlborn. 2018. Unmanned aerial vehicle (UAV)-based assessment of concrete bridge deck delamination using thermal and visible camera sensors: A preliminary analysis. *Research in Nondestructive Evaluation*, Vol. 29, No. 4, pp. 183–198. https://doi.org/10.1080/09349847.2017.1304597.

Feroz, S., and S. Abu Dabous. 2021. UAV-based remote sensing applications for bridge condition assessment. *Remote Sensing*, Vol. 13, No. 9. https://doi.org/10.3390/rs13091809.

Fischer, S., J. Lu, K. Van Fossen, and E. Lawless. 2020. *Global Benchmarking Study on Unmanned Aerial Systems for Surface Transportation: Domestic Desk Review*. Federal Highway Administration, Washington, DC. https://rosap.ntl.bts.gov/view/dot/54181%0A.

Flammini, F., C. Pragliola, and G. Smarra. 2016. Railway infrastructure monitoring by drones. International Conference on Electrical Systems for Aircraft, Railway, Ship Propulsion and Road Vehicles and International Transportation Electrification Conference (ESARS-ITEC), November 2–4, Toulouse, France.

Hubbard, S., A. Pak, Y. Gu, and Y. Jin. 2017. UAS to support airport safety and operations: Opportunities and challenges. *Journal of Unmanned Vehicle Systems*. https://doi.org/10.1139/juvs-2016-0020.

Leonardi, G., V. Barrile, R. Palamara, F. Suraci, and G. Candela. 2019. Road degradation survey through images by drone. *International Symposium on New Metropolitan Perspectives*, pp. 222–228. Springer, New York, NY. https://doi.org/10.1007/978-3-319-92102-0_24.

McGuire, M., M. J. Rys, and A. Rys. 2016. *A Study of How Unmanned Aircraft Systems Can Support the Kansas Department of Transportation's Efforts to Improve Efficiency, Safety, and Cost Reduction*. Report No. K-TRAN: KSU-15-3. Kansas Department of Transportation, Topeka, KS.

Moon, B., and H. Lee. 2022. Drone-image based fast crack analysis algorithm using machine learning for highway pavements. *Engineering Proceedings*, Vol. 17, No. 1, pp. 15.

Nooralishahi, P., C. Ibarra-Castanedo, S. Deane, F. López, S. Pant, M. Genest, N. P. Avdelidis, and X. P. V. Maldague. 2021. Drone-based non-destructive inspection of industrial sites: A review and case studies. *Drones*, Vol. 5, No. 4, pp. 106. https://doi.org/10.3390/DRONES5040106.

Peddinti, P. R. T., H. Puppala, and B. Kim. 2023. Pavement monitoring using unmanned aerial vehicles: an overview. *Journal of Transportation Engineering, Part B: Pavements*, Vol. 149, No. 3.

Pietersen, R. A., M. S. Beauregard, and H. H. Einstein. 2022. Automated method for airfield pavement condition index evaluations. *Automation in Construction*, Vol. 141. https://doi.org/10.1016/J.AUTCON.2022.104408.

Pokhrel, R., R. Samsami, S. Elmi, and C. N. Brooks. 2024. Automated concrete bridge deck inspection using unmanned aerial system (UAS)-collected data: A machine learning (ML) approach. *Eng*, Vol. 5, No. 3, pp. 1937–1960.

Quinton, D., and T. J. Regan. n.d. *Use of Unmanned Aerial Systems (UAS) by State DOTs: February 27, 2018 Peer Exchange*. Federal Highway Administration, Washington, DC. https://rosap.ntl.bts.gov/view/dot/43679.

Roberts, R., L. Inzerillo, and G. Di Mino. 2020. Using UAV based 3D modelling to provide smart monitoring of road pavement conditions. *Information*, Vol. 11, No. 12, pp. 568.

Sattar, S., S. Li, and M. Chapman. 2018. Road surface monitoring using smartphone sensors: A review. *Sensors*, Vol. 18, No. 11.

Seo, J., L. Duque, and J. Wacker. 2018. Drone-enabled bridge inspection methodology and application. *Automation in Construction*, Vol. 94, pp. 112–126. https://doi.org/10.1016/j.autcon.2018.06.006.

Sourav, M. A. A., H. Ceylan, C. Brooks, R. Dobson, S. Kim, D. Peshkin, and M. Brynick. 2024a. Use of small unmanned aircraft systems in airfield pavement inspection: implementation and potential. *International Journal of Pavement Engineering*, Vol. 25, No. 1.

Sourav, M. A. A., H. Ceylan, C. Brooks, D. Peshkin, S. Kim, R. Dobson, C. Cook, M. Mahedi, and O. Brouillette. 2022a. *Small Unmanned Aircraft System for Pavement Inspection: Task 4—Execute the Field Demonstration Plan and Analyze the Collected Data*. Federal Aviation Administration, Washington, DC. https://doi.org/https://doi.org/10.21949/1524511.

Sourav, M. A. A., H. Ceylan, C. Brooks, D. Peshkin, S. Kim, R. Dobson, C. Cook, M. Mahedi, and A. Jenkins. 2023. *Small Unmanned Aircraft System for Pavement Inspection*. Federal Aviation Administration, Washington, DC. https://doi.org/10.21949/1528226.

Sourav, M. A. A., H. Ceylan, C. Brooks, D. Peshkin, S. Kim, R. Dobson, A. Jenkins, and C. Cook. 2022b. *Practical Lessons Learned from Planning, Collecting, Processing, and Analyzing Small Unmanned Aircraft System Data for Airfield Pavement Inspection*. Federal Aviation Administration, Washington, DC.

Sourav, M. A. A., H. Ceylan, S. Kim, C. Brooks, D. Peshkin, R. Dobson, M. Brynick, and M. DiPilato. 2022c. Small uncrewed aircraft systems-based orthophoto and digital elevation model creation and accuracy evaluation for airfield portland cement concrete pavement distress detection and rating. International Conference on Transportation and Development, May 31–June 3, Seattle, WA. https://doi.org/10.1061/9780784484371.016.

Sourav, M. A. A., H. Ceylan, S. Kim, and M. Brynick. 2024b. Integration of small unmanned aircraft systems and deep learning for efficient airfield pavement crack detection and assessment. International Conference on Transportation and Development, June 15–18, Atlanta, GA.

Sourav, M. A. A., M. Mahedi, H. Ceylan, S. Kim, C. Brooks, D. Peshkin, R. Dobson, and M. Brynick. 2022d. Evaluation of small uncrewed aircraft systems data in airfield pavement crack detection and rating. *Transportation Research Record*, Vol. 2677, No. 1, pp. 653–668. https://doi.org/10.1177/03611981221101030.

Tan, Y., and Y. Li. 2019. UAV photogrammetry-based 3D road distress detection. *ISPRS International Journal of Geo-Information*, Vol. 8, No. 9. https://doi.org/10.3390/ijgi8090409.

Tomiczek, A. P., T. J. Whitley, J. A. Bridge, and P. G. Ifju. 2019. Bridge inspections with small unmanned aircraft systems: Case studies. *Journal of Bridge Engineering*, Vol. 24, No. 4. https://doi.org/10.1061/(ASCE)BE.1943-5592.0001376.

Vidyadharan, A., T. Carter, H. Ceylan, C. Bloebaum, K. Gopalakrishnan, and S. Kim. 2017. Civil infrastructure health monitoring and management using unmanned aerial systems. *Airfield and Highway Pavements 2017*, pp. 207–216. https://doi.org/10.1061/9780784480946.019.

Watts, A. C., V. G. Ambrosia, and E. A. Hinkley. 2012. Unmanned aircraft systems in remote sensing and scientific research: Classification and considerations of use. *Remote Sensing*, Vol. 4, No. 6, pp. 1671–1692.

THE INSTITUTE FOR TRANSPORTATION IS THE FOCAL POINT FOR TRANSPORTATION AT IOWA STATE UNIVERSITY.

InTrans centers and programs perform transportation research and provide technology transfer services for government agencies and private companies;

InTrans contributes to Iowa State University and the College of Engineering's educational programs for transportation students and provides K–12 outreach; and

InTrans conducts local, regional, and national transportation services and continuing education programs.

IOWA STATE UNIVERSITY

Visit **InTrans.iastate.edu** for color pdfs of this and other research reports.